# Multiscale viscoplastic modeling of recycled glass fiber-reinforced thermoplastic composites: Experimental and numerical investigations

M.Nachtane[1,2 *], F. Meraghni[1], G. Chatzigeorgiou[1], L. T. Harper[3], F. Pelascini[2]

[1]Arts et Métiers Institute of Technology, CNRS, Université de Lorraine, LEM3-UMR7239, 4 Rue Augustin Fresnel Metz, 57078, France

[2] Cetim Grand Est, 67400 Illkirch-Graffenstaden, France

[3] Faculty of Engineering, University of Nottingham, UK

Corresponding author: mourad.nachtane@ensam.eu

## Abstract

One of the main challenges facing fiber-reinforced polymer composites is the lack of options for end-of-life recycling. The environmental impact of waste materials disposed of at landfill sites, by incineration, or by erratic dispersion in the environment is accelerating the need to find innovative solutions to increase the value of recycled materials. This research aims to investigate the relationship between microstructural parameters and the mechanical properties of a recycled thermoplastic composite material. The latter is processed by thermocompression molding of a polyamide (PA66) matrix reinforced with chopped glass strands. An innovative approach is proposed to link the local microstructure of the composite to the mechanical behavior of the recycled material. It exploits an experimental characterization of the material microstructure using optical microscopy and X-ray micro-computed tomography (mCT). The experimental findings are implemented into a numerical modeling strategy to mimic the flexural behavior, based on a micromechanical approach coupling mean and full-field analysis. The region of interest is reconstructed from detailed 3D images using a modified random sequential adsorption (MRSA) algorithm, while other regions are modeled as homogenized macro-scale continua. Furthermore, the abilities of the proposed approach are proven by incorporating the viscoplastic behavior of the random heterogeneous material induced by the polymer matrix. The originality of the present research consists of the multi-scale FE analysis and the experimental validation for the viscoplastic behavior of the recycled composite material, taking into account influences from the microstructure.

**Keywords:** Recycled composite materials, Multiscale viscoplastic modeling, Microstructural analysis, Compression molding, Hybrid computational model.

# 1. Introduction

Thermoplastic materials offer great opportunities for mass production of fiber-reinforced composites and are being adopted across a large range of applications within the automotive, aerospace, construction, and renewable energy sectors [1]. Key advantages include high specific mechanical properties, low-cost raw materials, superior impact properties, and the potential to be reshaped or recycled by reheating [2], compared to thermoset equivalents. Recycling of thermoplastic composites has attracted substantial interest and is expected to become mandatory from an environmental perspective in the future. Composites recycling will not only reduce the negative impact on the environment but also minimize disposal costs and reduce the demand for virgin materials.

An essential aspect of the development of sustainable recycling technology is to identify the optimal recycling route for different types of composites. Thermoset polymer composites have a cross-linked structure upon moulding, with the inability to be reconstructed when heated (irreversibly destroyed cross-links). Current recycling approaches typically consist of mechanical, thermal, and chemical-based solutions, where the selection depends on the type of material to be recycled and the application in which the product it is to be reused [3, 4]. As far as the breakdown of recycling technologies of research and industry is concerned, solvolysis (24%), pyrolysis (31%) and mechanical grinding (18%) are characterized by the highest acceptance [5].

Thermoplastics including polyamide/Nylon (PA), polyethylene (PE), polyvinyl chloride (PVC) and polystyrene (PS), etc. are commonly recyclable. Mechanical recycling techniques involve the use of grinding techniques to comminute the scrap material and produce recycled products in different size ranges suitable for reuse as fillers or partial reinforcement in new composite material. This process is the most preferred and the least expensive for recycling glass fiber reinforced plastics [6]. Several parameters such as extruder speed and torque, mold temperature, some recycling process, etc. significantly affect the resulting mechanical properties of the recycled composite.

In this research, a mechanical process will be used for recycling glass fiber-reinforced Nylon66 matrix composites. However, the development of recycled thermoplastic composites has been limited by the lack of understanding about the durability of these materials. It is difficult to estimate the lifespan because of their heterogeneous mesostructure, but also because their mechanical performance is inextricably linked to the parameters used during the fiber

recovery stage and the subsequent processing parameters used during composite manufacturing. Henshaw et al. [7] analyzed the technical feasibility of recycling a cyclic polycarbonate-matrix continuous-glass-fiber composite by two common processes: compression molding and injection molding. This work indicated that injection molded parts exhibited good mechanical properties compared to compression molding, implying no adverse effects from the recycling process. However, compression molded recycled materials revealed relatively low properties compared to non-recycled materials, due to the heterogeneous fiber architecture following the recycling step. Colucci et al.[8] studied the mechanical behavior of recycled polymeric composites based on PA66 reinforced with short carbon fibers manufactured through injection molding. The recycling process had no significant effect on the microstructure or the final properties of the recycled composites. Recently, Kiss et al. [9] conducted an experimental investigation to understand the mechanical behavior of recycled sheet materials. It was concluded that the properties were insensitive to the fiber length (ranging from 5mm to 25mm), but the poor tensile, flexural, and impact responses were dominated by the fiber orientation distribution.

Mengeloglu et al. [10] investigated the thermal degradation, mechanical behavior, and morphology of recycled thermoplastic composites. The authors observed that the addition of maleated polyolefins as coupling agents had a considerable impact and improved the mechanical properties regardless of polymer type, due to the improved adhesion. In addition, the mechanical properties of recycled composites are extremely sensitive to factors such as fiber length attrition, matrix-fiber interfacial strength, volume fraction, fiber orientation, and void content [11]. Barnett et al. [12] studied recycled discontinuous fiber thermoplastic matrix organosheet manufactured via compression molding. The void content of the composites was quantified by employing optical microscopy and density measurements. The void content of the recycled random fiber composite ($3.5 \pm 2.6$ %) was lower than that of the virgin fiber equivalent ($13.9 \pm 6.1$ %), which had a minor influence on the mechanical performance. Vincent et al. [13] developed a novel analysis technique to characterize the fiber length and fiber distribution in the recycled material based on images from batches of multi-layered flakes. Process and material-induced heterogeneities for the recycled thermoplastic composites are like those experienced for other long-fiber thermoplastics, including fiber orientation, volume fraction, and fiber length attrition.

Limited work has been performed using numerical simulations to predict the material properties of ROS (Randomly Oriented Strands) or ROF (Randomly Oriented Fiber)

composites, to support the development of recycled thermoplastics. Visweswaraiah et al. [14] presented a review of the mechanical characterization and modeling of ROS architectures and their hybrids. The numerical modeling techniques can be categorized into three groups: micro, meso, and macro models. Various algorithms have been employed to create the representative volume element (RVE) of ROS and ROF composites. In a meso-level model, Harper et al. [15] generated representative architectures for discontinuous fiber composites by employing a force-directed algorithm. Pan et al. [16] used a modified random sequential adsorption algorithm (MRSA) to generate the complex architecture of a random fiber composite and coupled it with a homogenization procedure to obtain the overall elastic properties. Tang et al. [17] established a new stochastic chip-packing algorithm for microstructure reconstruction of chopped carbon fiber chip-reinforce composites. In parallel, the authors proposed a multi-level progressive damage model to predict fatigue behavior. There was a good agreement between the numerical model and the experimental results in terms of the observed damage mechanisms. Harban et al. [18] developed a new stochastic finite-element modeling technique named the Stochastic Laminate Analogy for the certification of discontinuous fiber composites, founded on experimental investigation. Kravchenko et al. [19, 20] studied the structure-property interaction for a prepreg platelet molded composite, taking a step further to add the compression molding simulation, mesostructure generation, and tensile performance prediction. At the macro-level, the multi-scale model was executed within a 3D finite element (FE) framework utilizing ABAQUS. Kilic et al. [21] presented a nonlinear 3D micromechanical framework to analyze discontinuous long-fiber thermoplastic composites. Their proposed framework shows an excellent predictive capability for the nonlinear behavior and global response of the discontinuous long-fiber (DLF) composites. Despite these efforts, hybrid meso-macro computational modeling for predicting the bending behavior of composites manufactured by ROS remains immature.

To gain a better understanding of the links between the microstructure and the mechanical behavior of recycled panels and products, a novel procedure for characterizing the mechanical response of recycled glass fiber-reinforced PA66 composites is presented in this paper. The bending behavior is predicted by using a new numerical modeling strategy that considers two zones: a specified zone of interest and a homogenized macro-scale zone. This approach depicts the global response by taking into account the influence of the local microstructure induced by the thermocompression moulding process.

The polyamide matrix is highly sensitive to water uptake, which governs the glass transition temperature as well as the rheology and damage mechanisms [22-26]. Specifically, this research focuses on the characterization of the microstructure and the global bending response using a hybrid computational model considering the elastic-viscoplastic response of the semi-crystalline matrix at 50% of relative humidity (RH50%) and room temperature (T=23°C). The modeling strategy adopted in this work is driven by the process-induced microstructure, accounting for the rate-dependent matrix response.

In summary, the outline of this article is as follows: Section 2 provides the material description and microstructural investigation as well as the recycling process, followed by the experimental methodology utilized for the mechanical characterization in Section 3. Section 4 covers the nonlinear modeling strategy and numerical simulation. Section 5 draws pertinent conclusions as well as some prospects for future developments.

# 2. Material description and microstructural investigation

## 2.1 Materials and recycling process

In approximately 90% of all cases, current production offcuts of thermoset and thermoplastic composites, as well as the end-of-life composite components, are not recycled. Following the European environmental directives, this makes the future use of fiber-reinforced composites a great concern. An innovative recycling process based on shredding has been developed by the research and technology organization (RTO) Cetim Grand Est, to preserve the added value of these materials, in particular their mechanical performance, and potentially improve them by providing additional functionalities compared to conventional non-recycled materials. (Figure 1) [27].

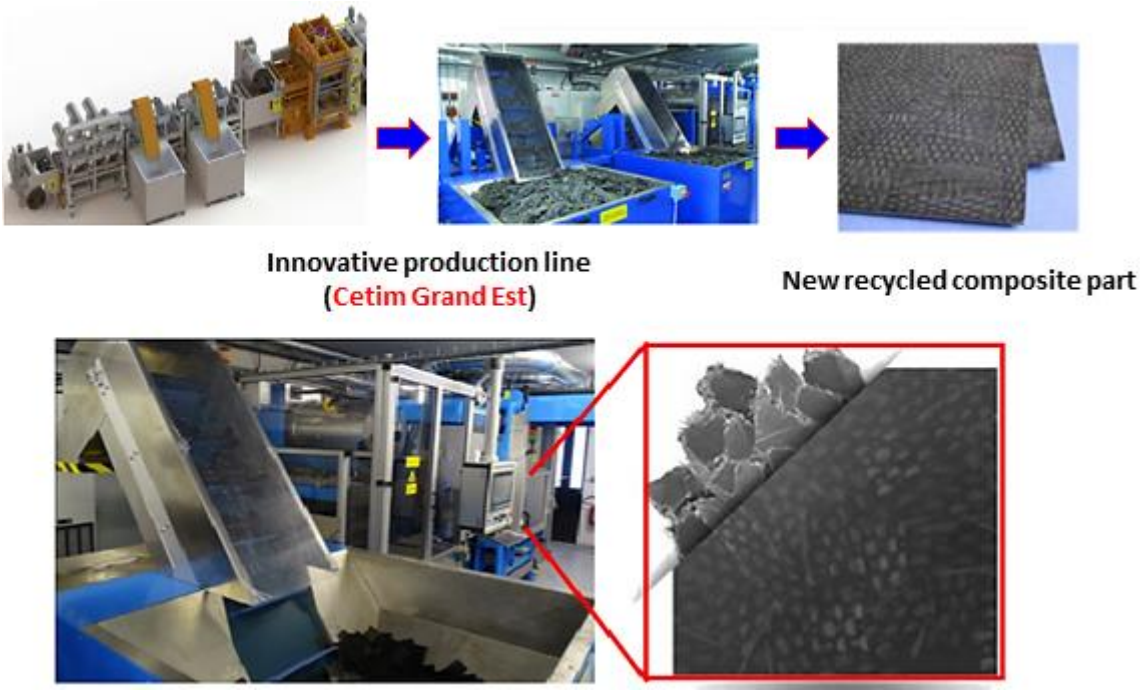


Figure 1: Cetim pilot line for recycling thermoplastic composites

Tepex® Dynalite (102-RG600(x)/PA-GF) is a consolidated composite laminate, based on a Polyamide 6 (PA6) matrix, which was manufactured and supplied by Bond-Laminates GmbH (Am Patbergschen Dorn 11-D-59929 Brilon, Germany). This material was shredded into 11–45 mm long pieces and then compression molded using an innovative modular production line developed by Cetim Grand Est, called a Thermosaic® line, as depicted in Figure 2. The material was pressed in two stages. The first pressure device is called the "contact press", which enables pre-heating and pre-compaction of the strands. The applied load during this initial step does not exceed 50 kN. In the second stage, the material is heated and compressed at the same time. The second press consists of a heating zone to melt the strands together and a cooling zone to freeze them into a plate. The maximum load (P) that can be applied here is 1300 kN. Finally, the recycled plate is ejected at the end of the line, as shown in Figure 2. - In this research, the process parameters were T=220-280°C and P=850-1000 kN.

There are numerous parameters, such as volume fraction, strand size, temperature, pressure, etc., which make it difficult to optimize the mechanical properties of recycled glass fiber-reinforced Nylon66 matrix composites without the aid of simulation. A multi-scaled approach considering the multi-physical couplings with the recycling process makes it possible to link the behavior of the microstructural constituents to the macroscale behavior of the recycled material. The originality of the present research resides in the development and experimental validation of a new modeling strategy that accounts for i) the effects induced by

the complex microstructure and ii) the elastic-viscoplastic behavior of recycled glass fiber-reinforced thermoplastic composite.

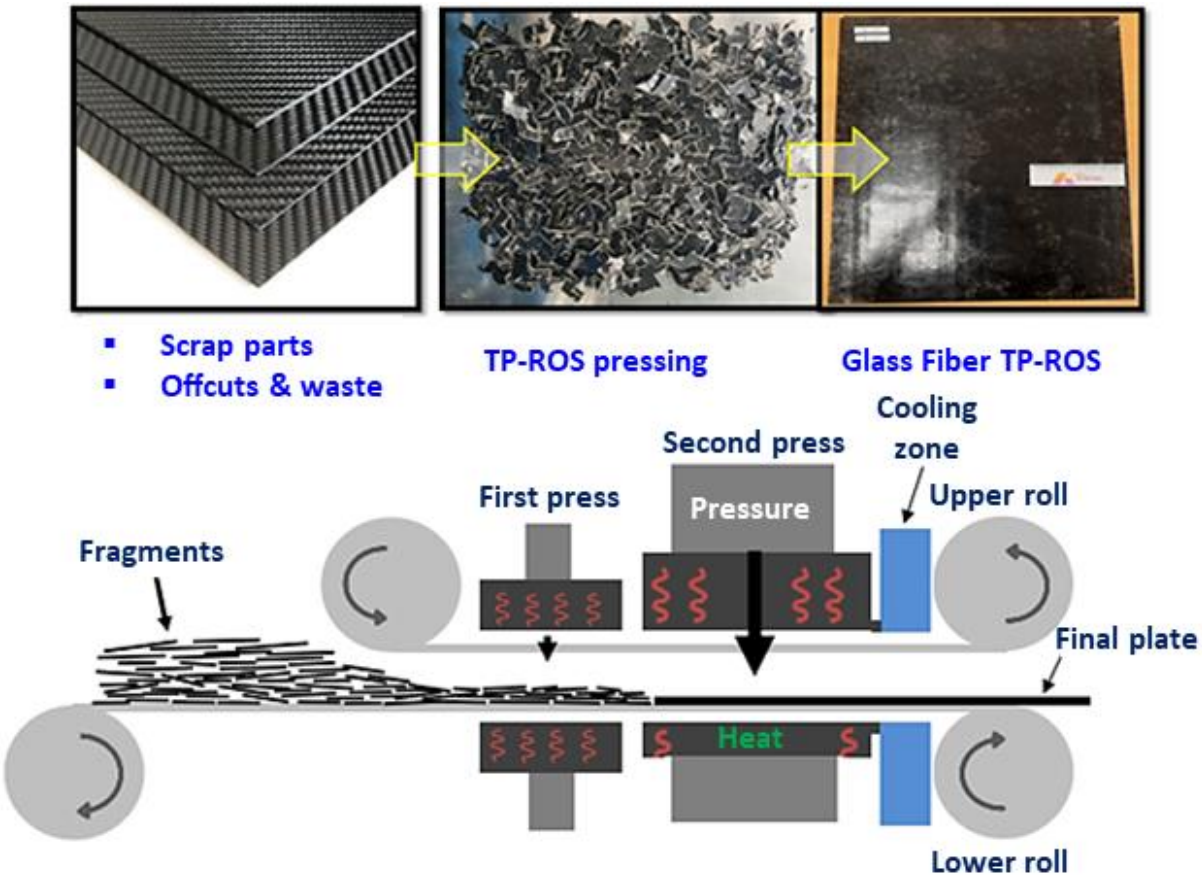


Figure 2: Industrial production line for recycling thermoplastic polymers

## 2.2 Microstructural analysis

The microstructural analysis is a vital stage in the "Processing-Microstructure-Property" framework for computational materials and design [28, 29]. A diverse range of simulation techniques and models has been established in the literature to generate microstructural models for the prediction of material properties [30], but unfortunately, they do not wholly capture the complex microstructural architecture of TP-ROS composites (e.g., spatial dispersion of fiber strands), because of the uncontrolled deposition and local material flow effects that occur during compression molding (see Figure 3). Zones exist within the material containing high fiber content interspersed with a zone of very low fiber content. Suitable descriptions of the internal geometry of this material for reliable mechanical property prediction require the acquisition and examination of huge quantities of data. For composites with ROS, the fiber orientation distribution can be described at two levels: (1) distribution of the fibers within the strands (micro-scale) and (2) the orientation of the strands (meso-scale). To address this issue, this

research aims to establish a microstructure-founded analysis technique to determine the strand morphology.

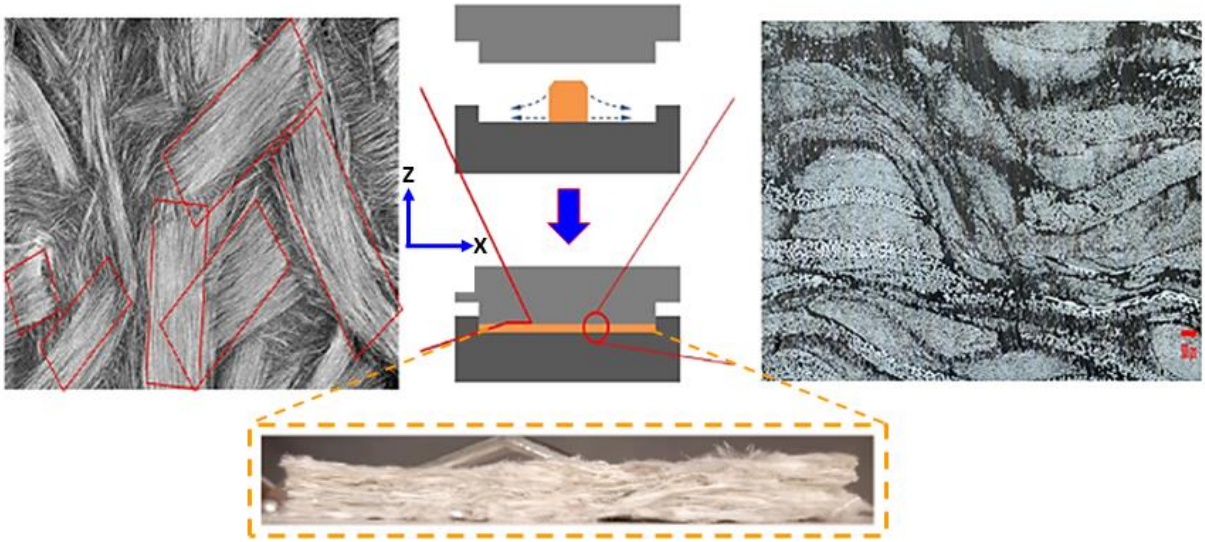


Figure 3: Interaction of strand chips during manufacturing

## a) Volume fraction measurement

To determine the glass fiber volume fraction of the recycled composite material, several samples have been subjected to the calcination process (Figure 4). The latter has been conducted within an oven at a temperature of 300°C for 24 hours. Specimens have been placed on a pre-weighed steel plate and the mass of the sample has been calculated before and after the test to a precision of 0.001g. Using this information, the mass fraction of the different phases of the composite are retrieved.

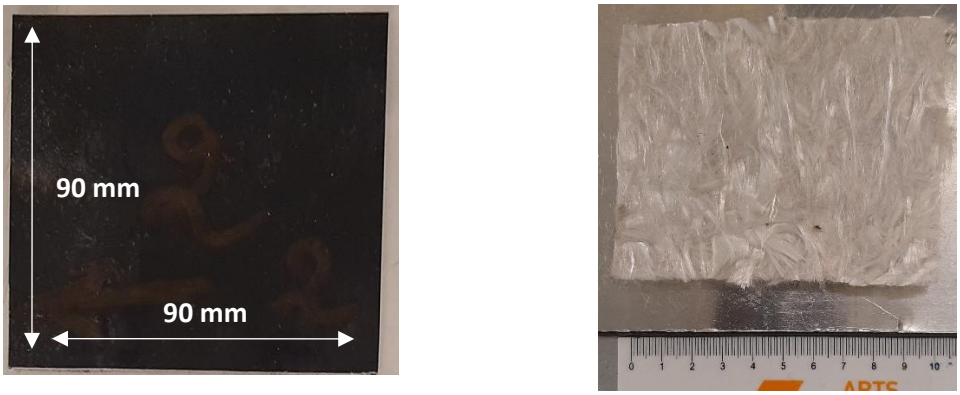


(a) before calcination (b) after calcination

Figure 4: Calcination of the recycled TP-ROS composites

From the density values of the Polyamide 66 and the glass fibers, the volume fraction of the fibers is calculated by equations (1 and 2), assuming the void ratio is zero. Table 1 presents the results of the calcination process.

$$M_f = \frac{A}{B} \times 100\% \quad (1)$$

$$V_f = \frac{M_f \rho_m}{\rho_f - M_f(\rho_f - \rho_m)} \times 100\% \quad (2)$$

With

- A: Weight of the sample in (g) after calcination (weight of fiberglass).
- B: Weight of the sample in (g) before calcination.
- $M_f$ and $M_m$ : Mass fraction of fiber and matrix in (%).
- $V_f$ and $V_m$: Volume fraction of fiber and matrix in (%).
- $\rho_f$ and $\rho_m$: Density of the matrix and the fiber (g/cm3)

Table 1: fiber volume and mass fractions

| | Mass fraction | Volume fraction |
|---|---|---|
| Sample 1 | 63.65% | 48.05% |
| Sample 2 | 63.42% | 47.80% |
| Average | **63.53%** | **47.92%** |

The most widely used technique to quantify the fiber length of random composite materials is to perform calcination, coupled with image analysis and processing. Measurements have been performed on a calcined Thermosaic® sample by recovering the fiber strands and arranging them on a plane. The length measurements have been achieved on 101 fiber strands as shown in Figure 5 (a). The curve in Figure 5 (b) shows the length distribution of the fibers following a normal distribution. It has been found that the average length of the fibers is 26.31 mm with a standard deviation of 7.33 mm.

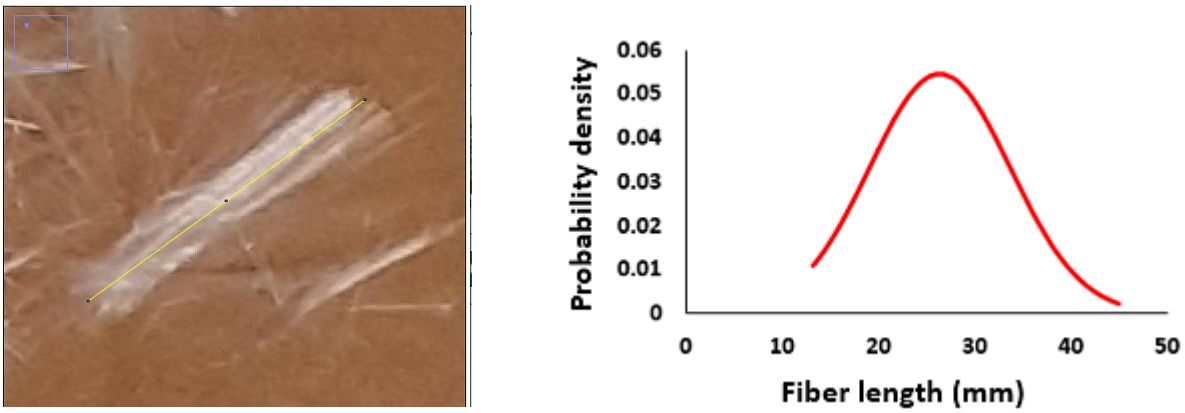


(a) (b)

Figure 5: fiber length distribution

## b) Optical (Light) Microscopy

The surfaces for microscopy were smoothed by a traditional technique using Mecaprex KM-U cold mounting resin, then polished by an automatic polishing machine (Figure 6). This procedure had to be conducted carefully to avoid any relief differences between the glass fibers and the matrix. In addition, the polishing time had to be as short as possible, employing a large flow of fresh water to avoid filling the voids with dust. Figures (6-a) and (6-b) show the evolution of the surface state between the two successive polishing steps. The acquisition of 168 micrographs with a resolution of 1.35 pixels/µm has been recorded. The corresponding images were then stitched together to form a single image using the AxioVision software.

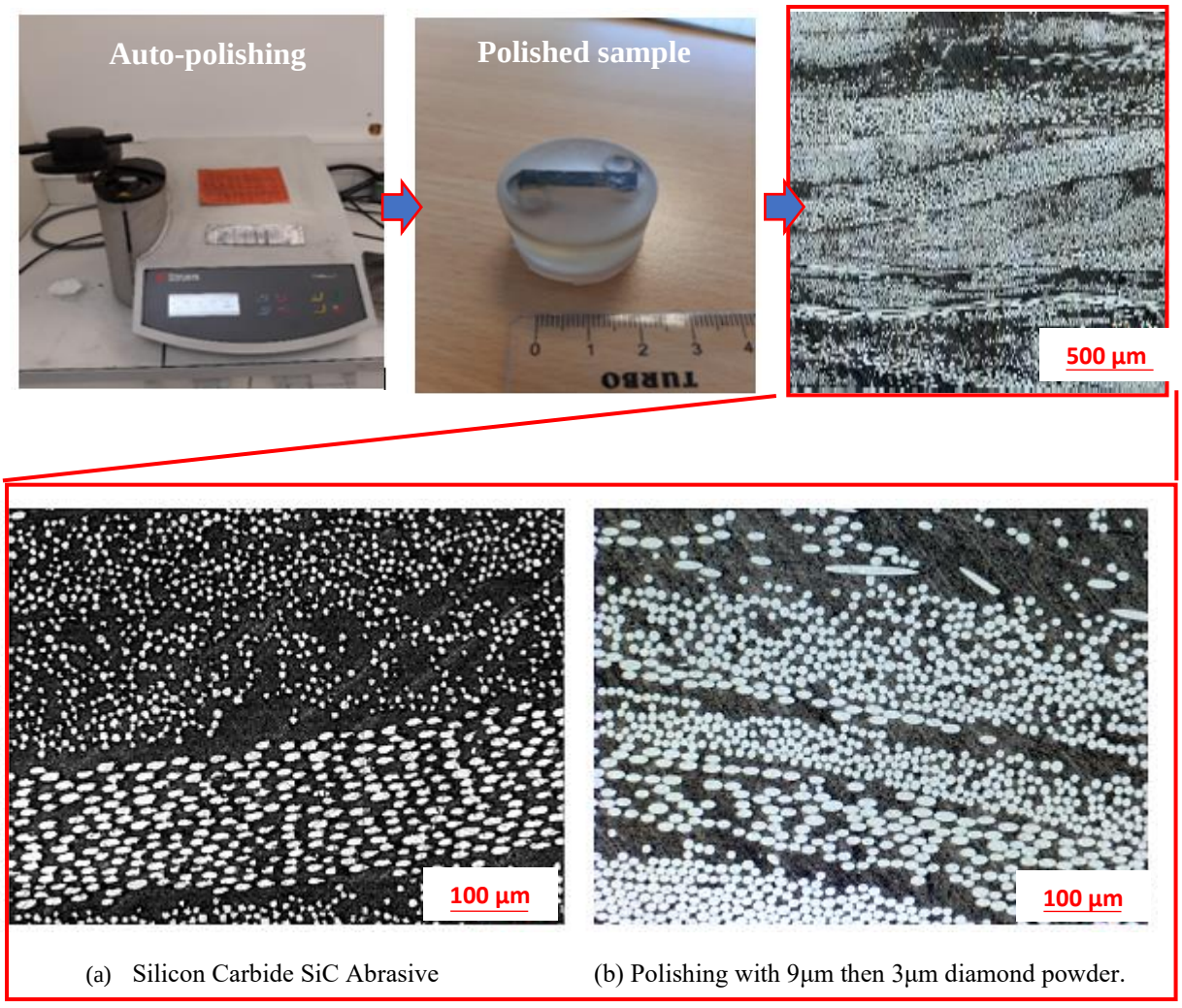


(a) Silicon Carbide SiC Abrasive (b) Polishing with 9µm then 3µm diamond powder.

Figure 6: Polishing steps and evolution of the surface state of recycled TP-ROS composites samples

Figure 7 shows the acquisition principle and the dimensions of the observed area. The post-processing of the micrographs has been accomplished with the ImageJ software.

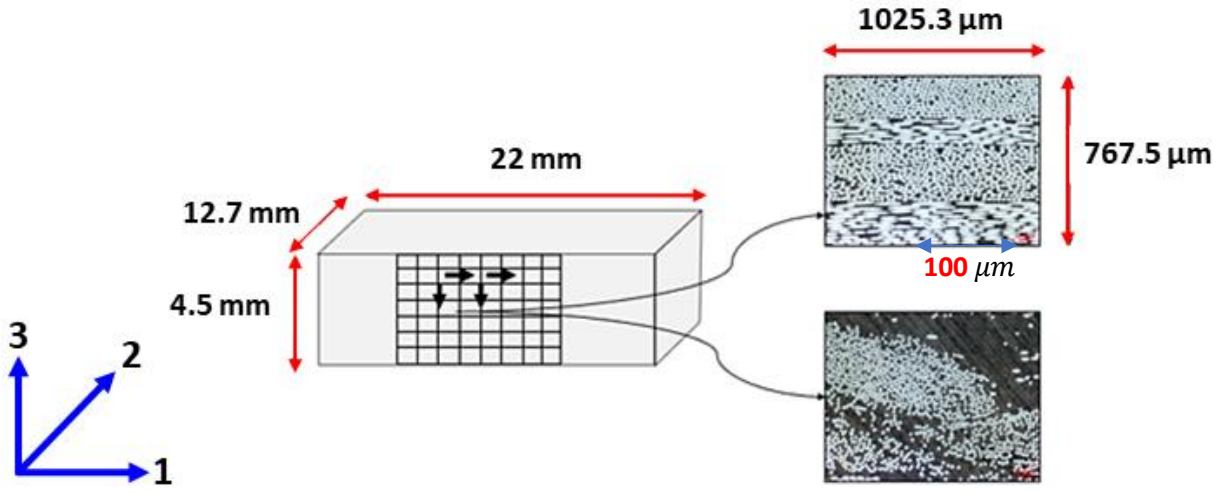


Figure 7: acquisition principle of sample micrographs

Microscopic observations showed the usual random microstructure of TP-ROS, with the presence of resin-rich zones and fiber-rich zones, as presented in Figure 8. The reconstructed images of the recycled TP-ROS composite material can be analyzed on two different scales:

- **At the microscopic scale,** the structure is homogeneous compared to the mesoscopic scale. Each strand contains fibers orientated similarly and dispersed homogeneously in a matrix solution. Two different strands can be distinguished by the presence of a matrix zone, or by a change in orientation of the fibers.
- **At the mesoscopic scale,** the structure consists of a high-density cluster of strands surrounded by resin-rich zones. These strands are mainly oriented in the plane, with a few strands inclined out-of-plane. This can be explained by the rheological behavior and the complicated flow phenomena of the woven ground materials during compression molding [31-33].

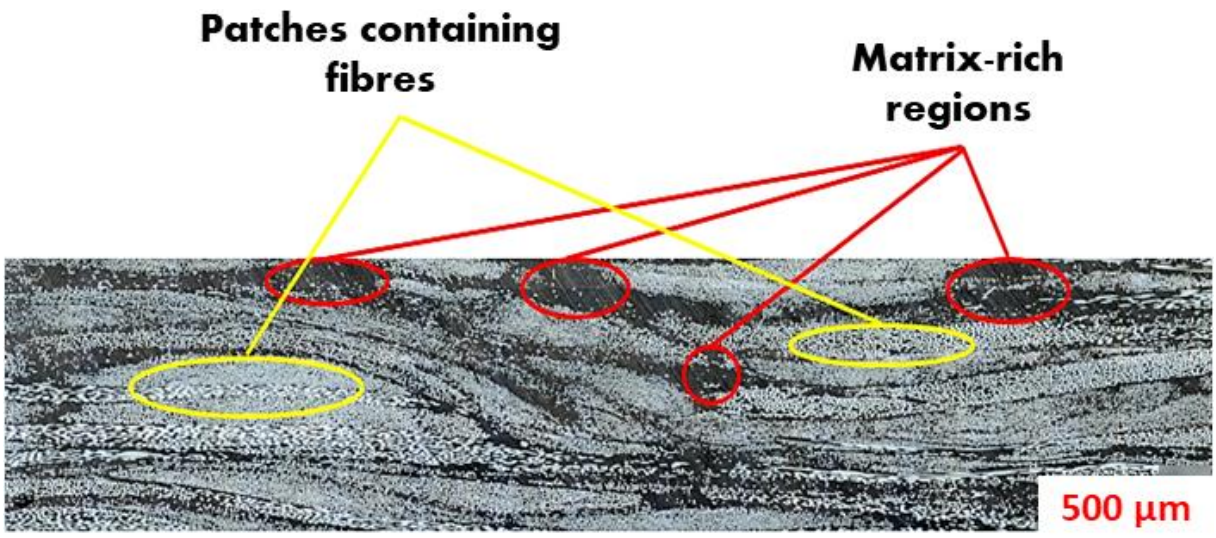


Figure 8: Complex morphology of TP-ROS

## c) X-ray Computed-Tomography analysis

X-ray micro-computed tomography (mCT) has become a valuable non-destructive technique for describing and quantifying structural features of composite materials [34-35]. TP-ROS composites generally have complex internal geometries due to the interaction of the strand chips and the effects of the processing parameters like temperature and pressure during the molding stage. To identify a representative sample of the TP-ROS material in terms of its structure, fiber

length, fiber volume fractions, and porosity, a compromise must be found between the analysis volume and the spatial resolution of the analysis.

Following the acquisition of the individual images, the data is post-processed using the X-Act software to remove defects and reconstruct the 3D model in a chosen direction. The images are transferred to 3D image viewing software, Avizo, where filters are applied to attenuate the noise. The median filter makes it possible to reduce the noise while keeping the contours of the image. It acts on each voxel of the reconstructed volume by replacing the value with the median value of the neighboring pixels. A volume of 18.70 x 17.80 x 4.5 $mm^3$ has been analyzed, which corresponds to a spatial resolution of 8.2 µm/pixel (Figure 9).

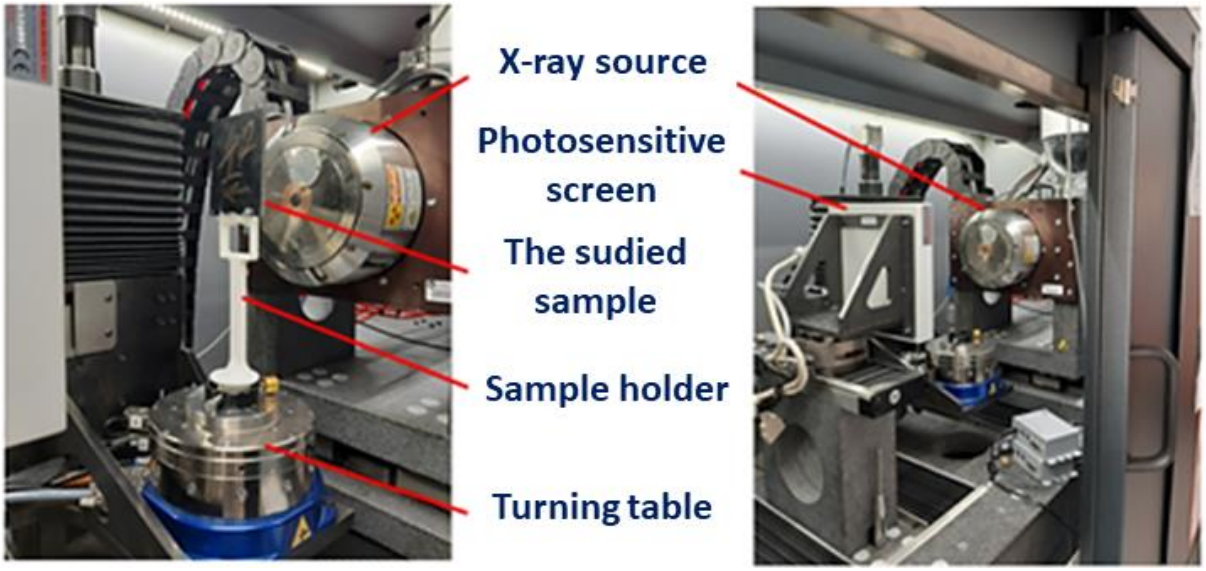


Figure 9: Experimental setup for analysis by X-ray tomography

X-ray tomography observations of the analyzed TP-ROS sample reveal a random microstructure of the TP-ROS material. Appropriate thresholding is then carried out to isolate each of the phases of the TP-ROS composite material, including matrix, fibers, and porosities as shown in Figure 10.

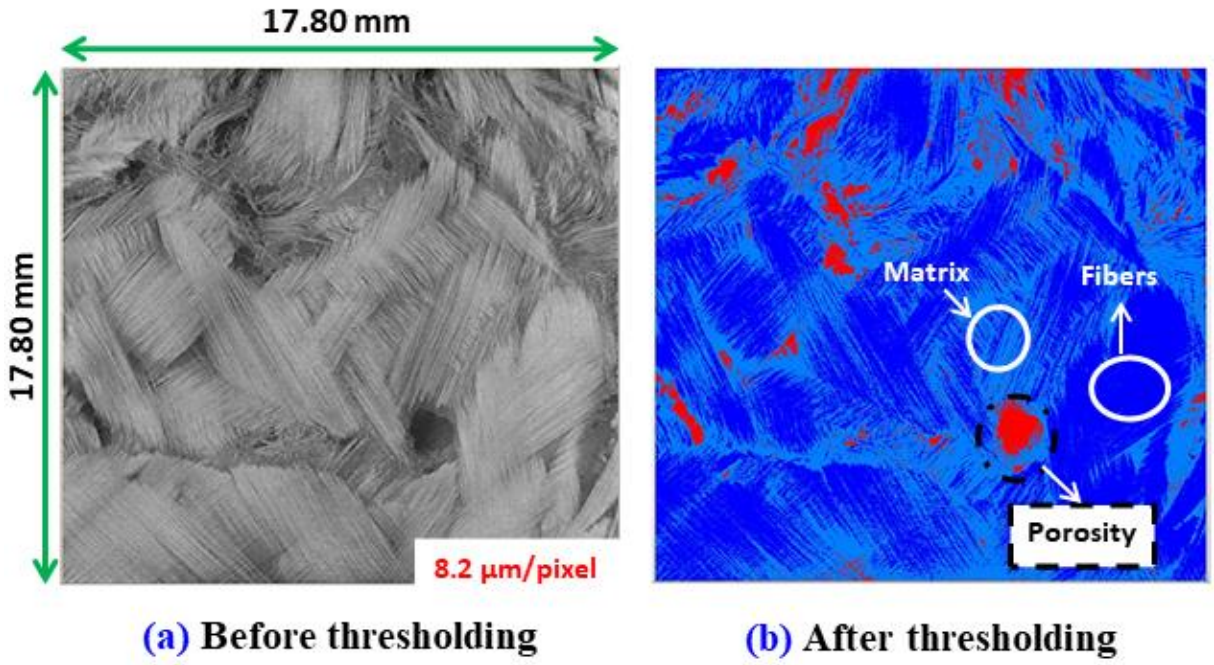


Figure 10: X-ray tomography images of a TP-ROS sample

The volume fraction of each of these phases can be quantified by calculating the number of voxels corresponding to a particular phase. Table 2 summarizes the results obtained for a sample of 18.70 x 17.80 x 4.5 $mm^3$. The results obtained by X-ray micro-tomography are in excellent agreement with the results found by the calcination process and confirm the overall fiber content value.

Table 2: Volume fractions of the different phases obtained by X-ray tomography.

| Fiber volume fraction | Matrix volume fraction | Porosity volume fraction |
|---|---|---|
| 45.52% | 50.73% | 3.75% |

## 3. Experimental methodology and results

To study the overall flexural response of the recycled glass fiber TP-ROS, a three-point bend test was carried out on a universal testing machine (Zwick Z050, Zwick-Roell, Germany) with a full-scale load of 50 kN. The loading procedure used the stroke velocity control mode (displacement controlled bending tests) at a constant value of 20 mm/min. The loading was applied through steel support rollers with a diameter of 10 mm, as shown in Figure 11(a). The dimensions of the three-point flexural test samples were 200 mm×40 mm×4.5 mm and the dimensions of the zone of interest was 40 mm×40 mm ×4.5 mm, as presented in Figure 11(b).

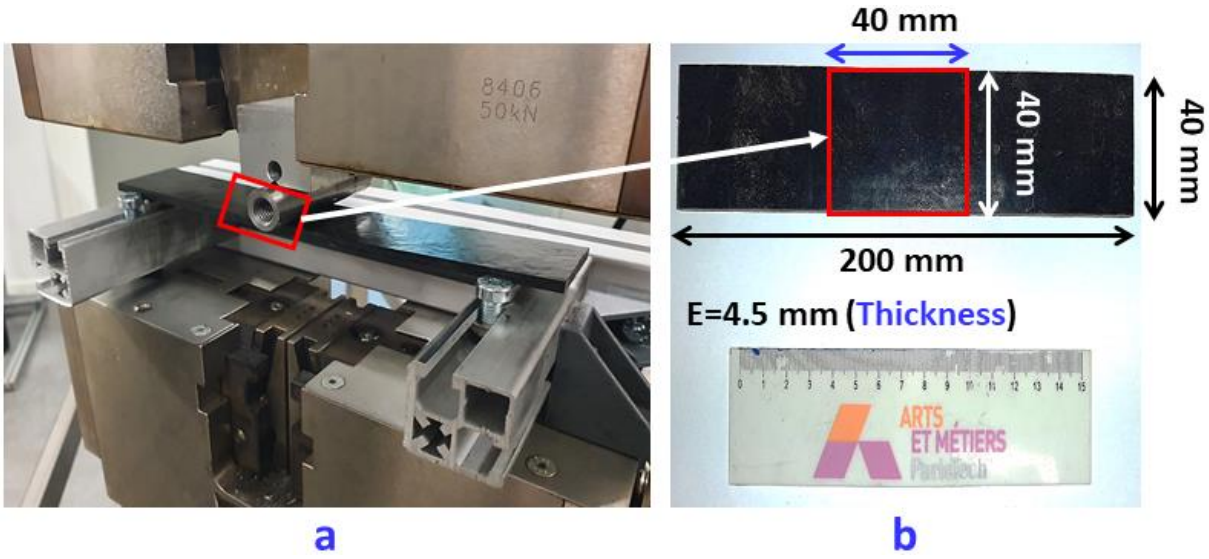


Figure 11: Three-point flexural test conducted using the Zwick Z050 universal testing machine.

The bending test was repeated four times for each specimen and the load-displacement curves of the recycled Glass fiber TP-ROS specimens are presented in Figure 12. The experimental load-displacement curves are generally repeatable, with the root mean square error being less than 8% for the four curves, demonstrating the robustness of the experimental procedure. Each curve can be divided into two zones. In the first zone, the load increases linearly with increasing displacement until it reaches approximately 348 N, corresponding to a displacement of 6.5 mm. After which, the curve becomes nonlinear due to the viscoplastic behavior of the matrix up until the sample fails due to the damage accumulation. This behavior is depicted in Figure 12, which implies that overall failure is matrix-driven. This type of behavior has also been observed by Selezneva et al [36,37], where damage initiation was observed in matrix-rich regions.

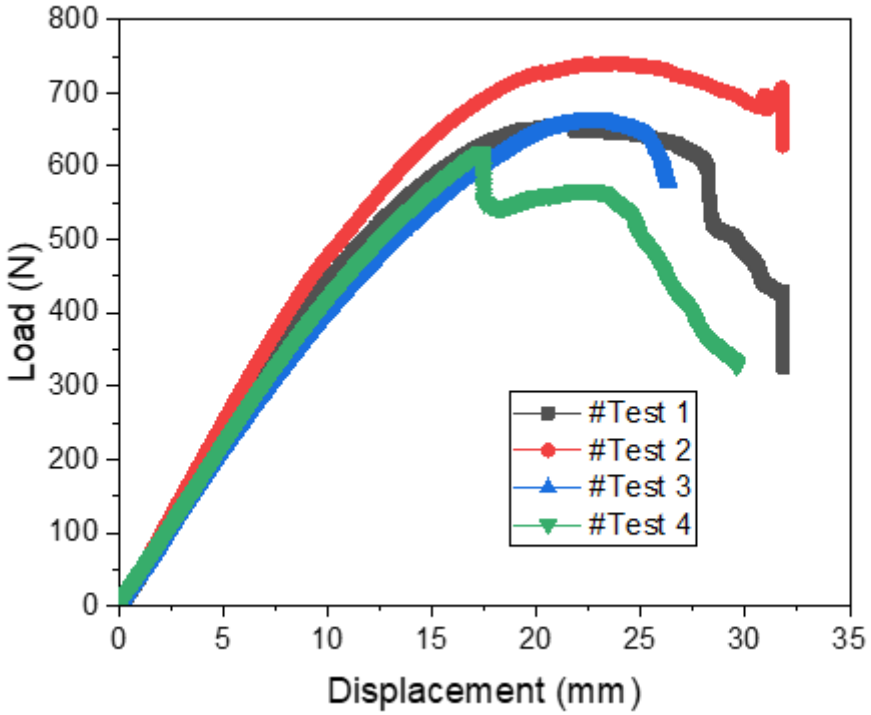


Figure 12: Load-displacement curve of TP-ROS specimens under bending test

Observations of the macroscopic damage have been analyzed to identify the failure modes for the recycled composite material, such as delamination, matrix cracks, and fiber breakage, as shown in Figure 13. The damage evolution is progressive: Firstly, the bottom surface of the sample fails in tension, driven by matrix cracking and fibers/matrix debonding. The damage then grows through the thickness. The crack is initiated from a matrix-rich zone on the upper part of the bent sample. The crack then propagates through the thickness of the sample, spreading around the boundaries of the strands. Delamination between strands is visible in inter-strand matrix-rich areas. The damage accumulation path connects stress concentrations that occur at the strand edges.

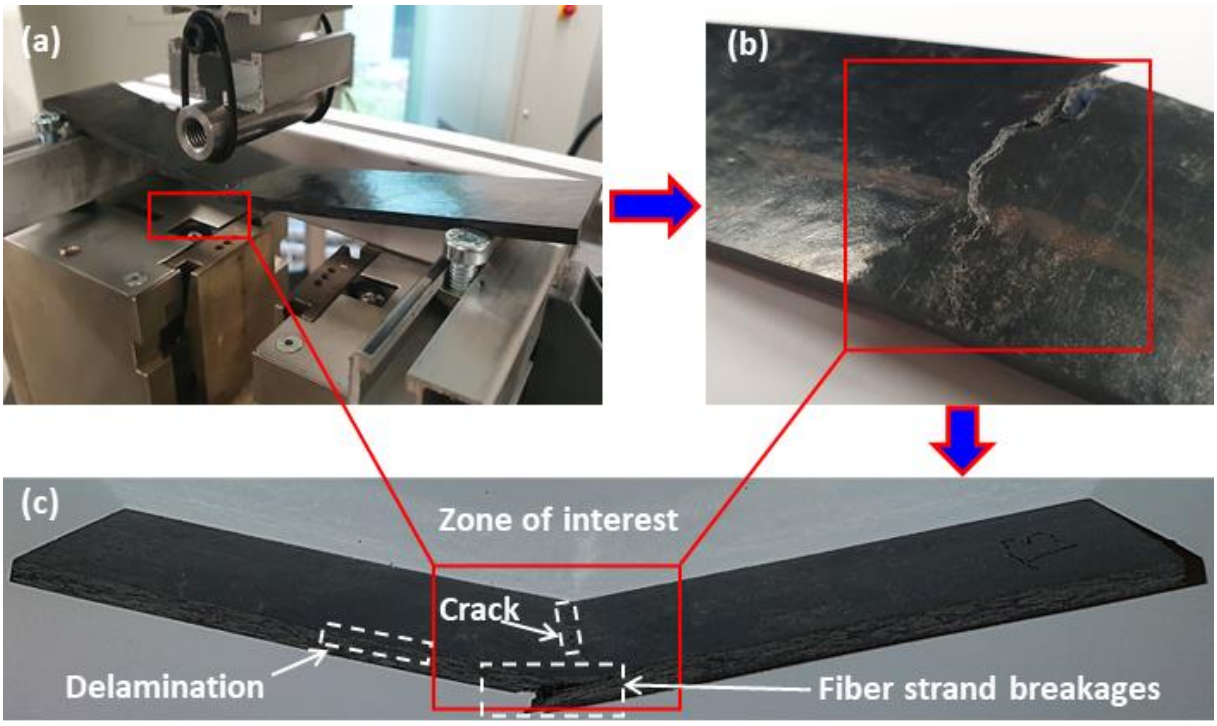


Figure 13: Failure modes in bending test

## 4. Nonlinear modeling strategy and numerical simulation

Based on the microstructure observations, the morphology of the recycled composite material is stochastic, or highly disordered, in the sense that the strands are arranged in "random" varying patterns, due to the uncontrolled deposition and local flow phenomenon that occurs during molding. This complex heterogeneous architecture affects the propagation of the complex damage paths, causing variability, which has prevented wider commercialization of these materials. It is therefore rational to develop an understanding of the material performance and extend mechanistic computational models to quantify the key process/structure/property interactions. The goal is therefore to diminish costly experimental testing programs and to facilitate design optimization.

### 4.1. Generation of mesoscopic RVEs

A simplified RVE model is proposed in this research, using a regular morphology for each of the strands, which can be beneficial for qualitative predictions of the effective overall performances of the studied composite. Based on the microstructural investigation presented in the previous sections, a much larger analysis volume has been defined to capture this material complexity, which is considered to be an RVE. Definitions of RVEs differ within the literature, but in the context of this research, it is considered to be a volume that is big enough to include many strands in the heterogeneous material, with the effective properties of the RVE

representing the macroscopic level of the real material, whilst remaining computationally inexpensive.

Realistic morphological characteristics must be reproduced in a virtual material morphology to provide rational and very accurate predictions of mechanical performance. The numerical model must integrate the strand size, the complex strand arrangement, and the variable strand orientation based on the microstructural observations. In this research, a realistic 3D representation of the recycled composite material is generated by an algorithm established by Harper et al [38]. This algorithm includes three steps. Firstly, a deposition algorithm is used to establish initial strand locations and orientations, to ensure the fiber volume fraction target for the RVE is met. Secondly, a force-directed method using an intersection-elevation mechanism is employed to identify and avert strand–strand intersections and to specify the through-thickness distribution of the strands. Thirdly, a spline interpolation algorithm is used to crop the smooth curved fiber strands to form the RVE boundaries. Finally, the reconstructed architecture is transferred to ABAQUS for FE analysis. The process flowchart of the RVE generation program is presented in Figure 14. Example RVE geometries (40×40×4.5mm) for different volume fractions are illustrated in Figure 15.

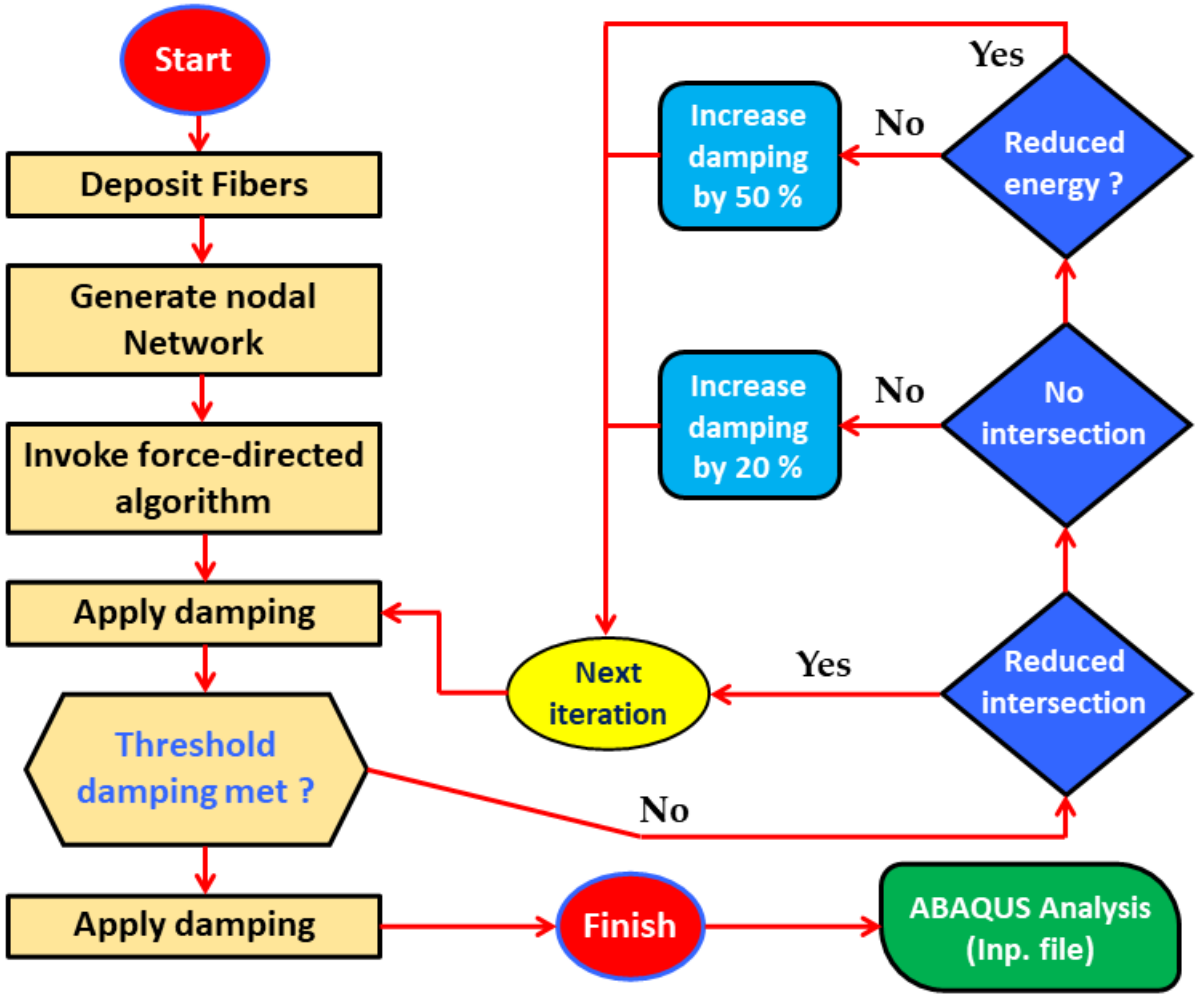


Figure 14: Flowchart for RVE generation


Figure 15: Example RVEs geometries (40 × 40 × 4.5 mm) for different volumes fractions

Internal morphological features, such as volume fraction, strand dimensions, and local structural distribution, define the global performance of the mesoscale heterogeneous strand-molded composite. Numerical models must therefore include these complex distributions to be realistic, but generating models with an appropriate fiber volume fraction is the principal limitation when producing RVEs for wholly stochastic architectures. Modified Random Sequential Adsorption (MRSA) algorithms are typically utilized to append consecutive fibers

to the RVE, eluding fiber–fiber intersections by removing contacting fibers. For this work, RVE geometries ($40\times40\times4.5mm^3$) containing rectangular fiber strands (26mm×14mm) are generated (Figure 15 (c)), which are physically representative of the fiber architectures observed by micro-computed tomography (Figure 16 (a) and Figure 16 (b)). The inputs for this RVE model consist of the geometrical parameters and the volume fraction of the strands.

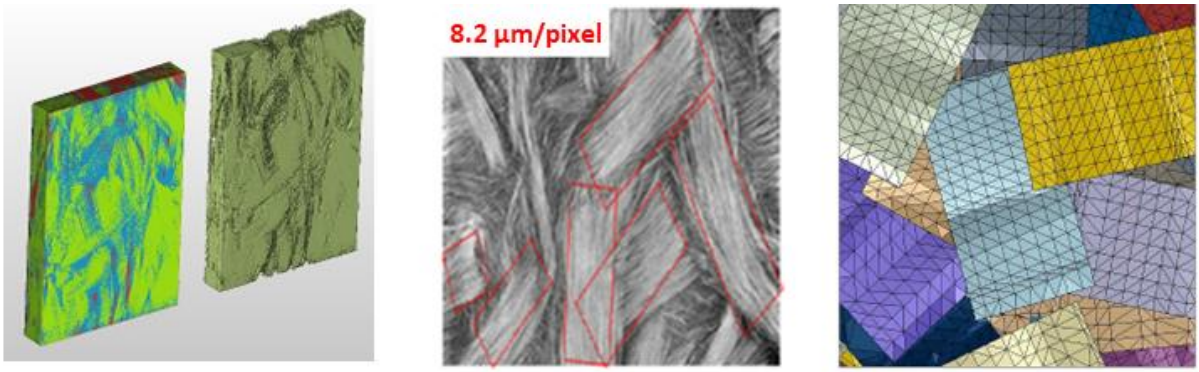


Figure 16: RVE geometries with rectangular fiber strand-based tomography observations

## 4.2 Multiscale modeling of three-point flexural test loading configuration

The TP-ROS has two distinct scales. At the mesoscopic scale, the structure consists of a high density of strands surrounded by a matrix skin, where the TP-ROS has a homogeneous appearance. On a microscopic scale, the density of fibers in the strand is greater at the core of the strand than at the periphery. The interval between two strands can be a single matrix area, a fiber concentration gradient, or it can be nonexistent. Figure 17 shows the hierarchical nature of a recycled composite obtained by the compression molding process.

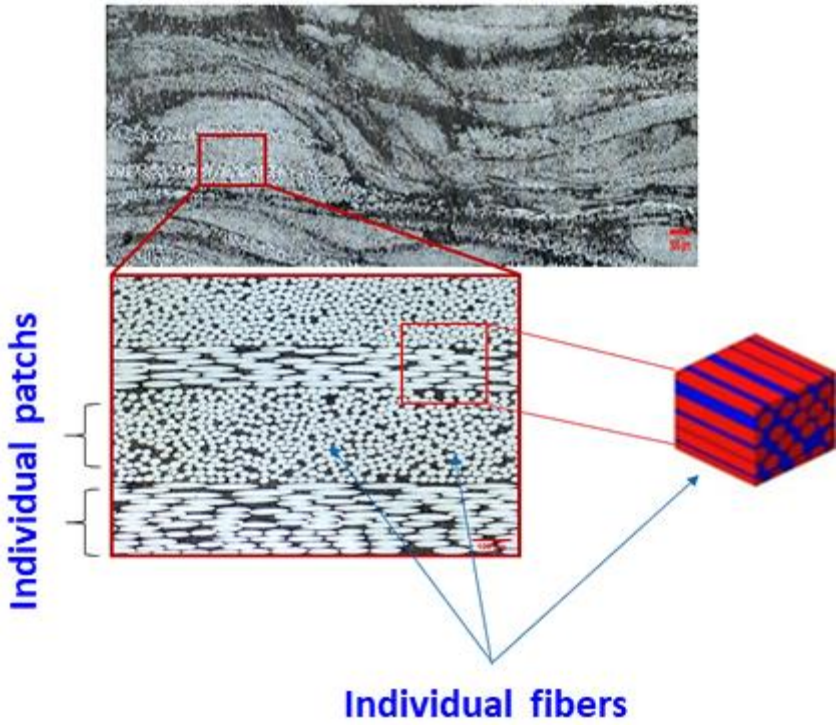


Figure 17: Hierarchical nature of a recycled composite from compression molding

A post-processing protocol is applied, based on the observable data. At the microscopic scale, the dominant microstructural parameters are the fiber volume fraction of the strand and the orientation of the fibers. While at the mesoscopic scale, additional parameters include the fiber volume fraction within the strand as well as the dimensions of the strands. From the micrographs obtained at the mesoscopic scale, the post-processing of the images stops at the binarization step. The strands are manually cropped. Once the contour of the strand is known, it is then possible to estimate the volume fraction of the fiber in these strands as well as their dimensions. This protocol is summarized in Figure 18.

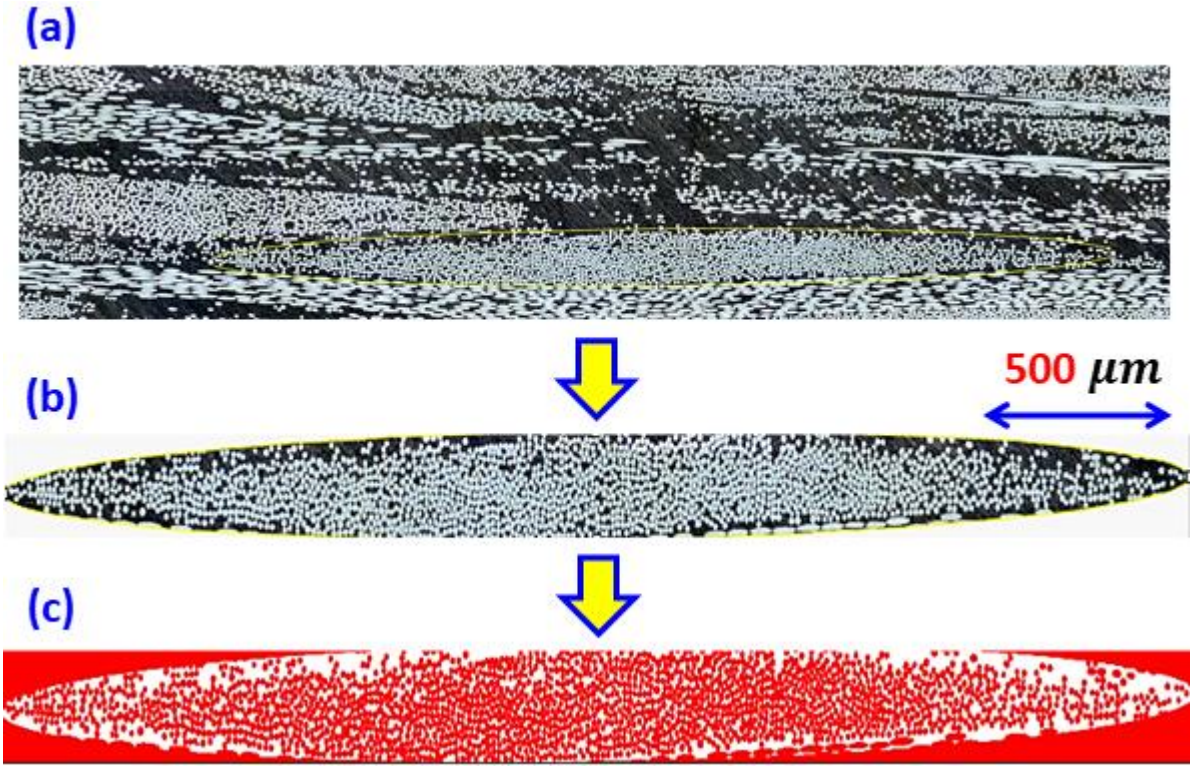


Figure 18: Protocol of volume fraction measurement

Knowing the overall volume fraction of fiber in the material (47%) and assuming that no porosity is present in the material, it is possible to calculate the volume fraction of the strand in the composite using equation (3):

$$\vartheta_{f/c} = \vartheta_{f/p} \times \vartheta_{p/c} \quad (3)$$

Where,

$\vartheta_{f/p}$: Volume fraction of fibers in a strand.

$\vartheta_{p/c}$: Volume fraction of the strands in the composite.

$\vartheta_{f/c}$: Volume fraction of fibers in the composite.

Table 4 presents the volume fractions at different scales of the TP-ROS composite:

Table 4: Volume fraction at various scales

| | Volume fraction (fibers/ strand) $\vartheta_{f/p}$ | Volume fraction (strand/ composite) $\vartheta_{p/c}$ |
|---|---|---|
| Average value | **81.03%** | **58.23%** |
| Standard deviation | 4.07% | 5.78% |

The modified RSA (MRSA) technique is employed to reconstruct the mesostructures of the TP-ROS material at the region of interest, which measures 40 mm × 40 mm × 4.5 mm. To represent the mechanical behavior of the strands, it is assumed that the fibers in each strand are oriented in the same direction, therefore the material properties of this analogous unidirectional (UD) composites can be calculated using a mean-field homogenization technique, such as a Mori-Tanaka scheme [39,40]. Away from the region of interest, other regions of the sample are considered to be homogenized continua to reduce the calculation time. The non-linear mechanical behavior (macro-scale model) is introduced in tabular form based on the performed experiments. It is noted that the experimentally obtained curve corresponds to isotropic in-plane behavior. Out of plane, the thickness of the specimen is small compared to the other dimensions. As a first approximation, the homogenized continua outside the zone of interest is assumed to be isotropic, due to a lack of additional information about the out-of-plane response of this material. This hypothesis relies on the fact that elastic homogenization on these zones provides Young moduli in the three directions with values of the same order of magnitude. Figure 19 presents a summary of the multi-scale modeling approach.

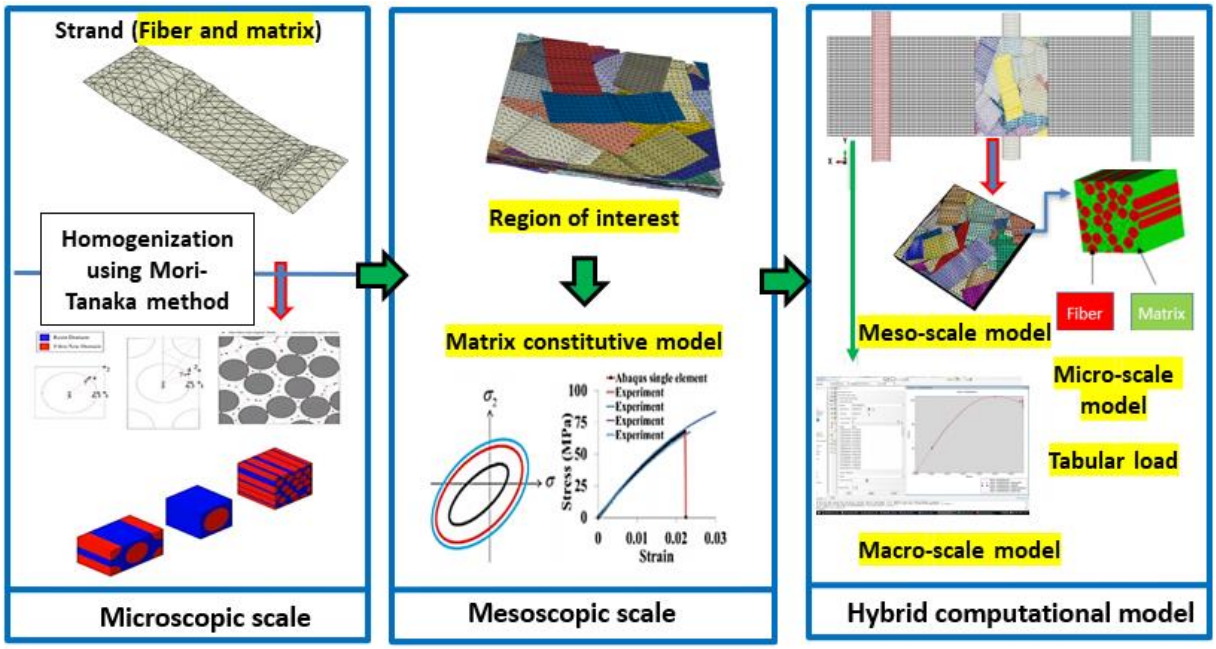


Figure19: Computational framework for multi-scale modeling of three-point flexural simulation

The representative computational model for the simulation of the three-point bend test is presented in Figure 20, where the various colored stripes depict the glass fiber strands and the red zone represents the polyamide matrix.

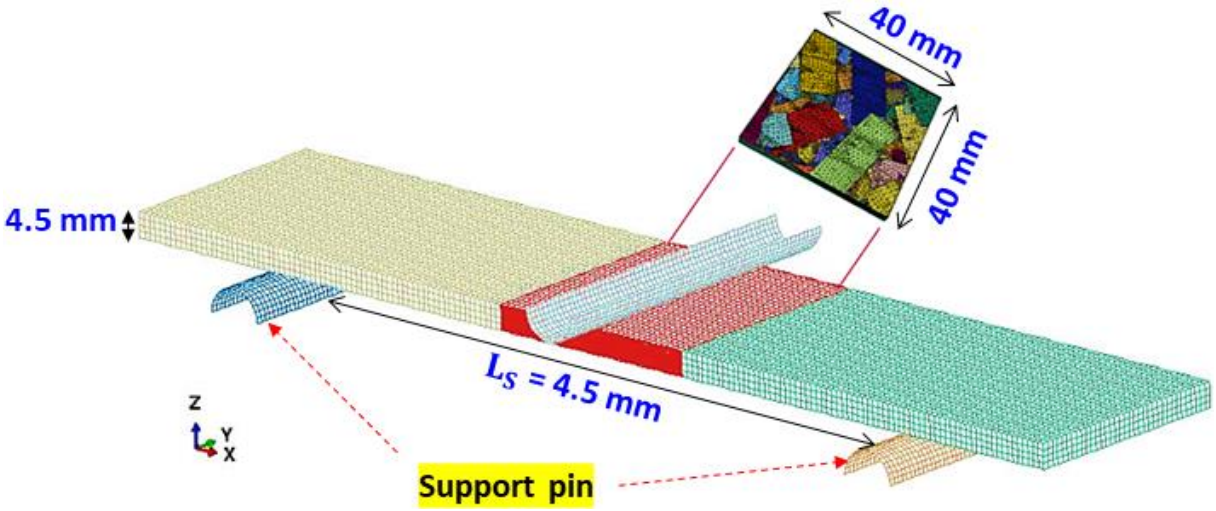


Figure 20: Representative computational model for three-point flexural test simulation of TP-ROS composite.

In the mesoscale model, the matrix material is discretized by employing continuum quadrilateral elements (C3D8). Shell elements (STRI65) depicting the fiber strand are attached to the continuum elements using the *EMBEDDED ELEMENT approach [41,42], which is used to specify that a group of strands is embedded in "host" elements representing the bulk matrix material. The translational degrees of freedom at the nodes of the embedded shell elements (strands) are specified by the translational degrees of freedom of the nodes of the host continuum elements (matrix). The green and yellow areas outside of the region of interest are the homogenized regions of TP-ROS composites, using 3D hexahedron elements (C3D8) in ABAQUS 6.20. The length of the full model is 200 mm. A rigid body element with 4 nodes (R3D4) was used to model the support and loading pin, with a diameter of 10 mm.

## 4.3 Experimental-numerical results comparison

To determine the mechanical properties of the strand, the Mori-Tanaka scheme has been adopted, assuming elastic glass fibers within each strand are aligned in a similar direction. In the work of Praud et al [43-45], a viscoelastic, viscoplastic model combined with ductile damage was proposed to describe the mechanical behavior of the thermoplastic matrix (PA66) under different loading configurations (monotonic, creep, cyclic, load/unload conditions). In the present work, where the study focuses only on uniaxial monotonic loading, a simplified model can be adopted, accounting for an elastic-viscoplastic response. Figure 21 presents a rheological representation of the elastic-viscoplastic behavior. The adopted elastic-viscoplastic

model accounts for the rate-dependent behavior considering the additive viscosity-hardening constitutive law of Chaboche (1989) and Chaboche (2008) [46-48]. This simplified model is adopted in the present work and the corresponding nonlinear constitutive law can be directly found within the ABAQUS library, or it can be easily implemented utilizing a Fortran User Material (UMAT) subroutine.

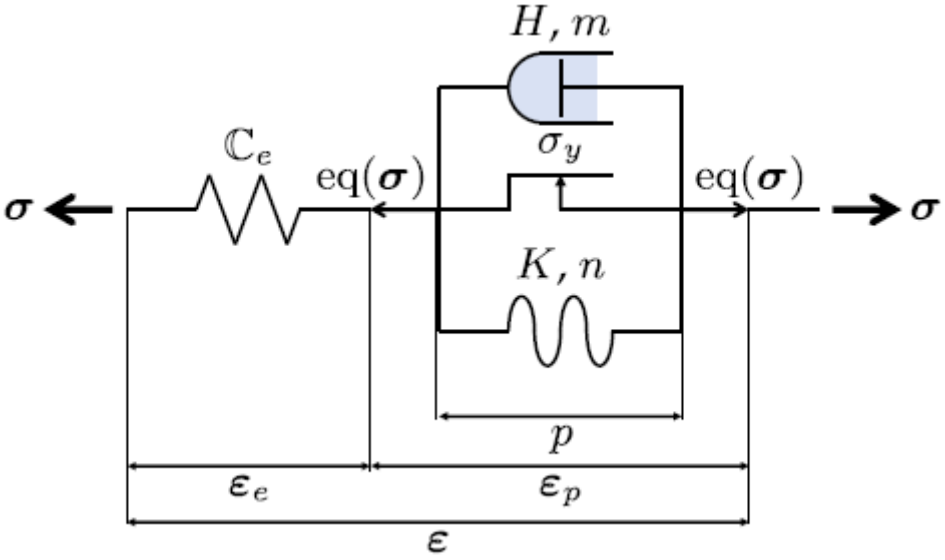


Figure 21: Schematic representation of the simplified elastic-viscoplastic model adopted for the PA66

The viscoplastic strain tensor $\boldsymbol{\varepsilon_p}$, the total strain tensor $\boldsymbol{\varepsilon}$, and the stress tensor $\boldsymbol{\sigma}$ are connected through the relation:

$$\boldsymbol{\sigma} = \boldsymbol{C}:(\boldsymbol{\varepsilon} - \boldsymbol{\varepsilon_p}), \tag{4}$$

where $C$ is the usual isotropic elasticity fourth-order tensor.

Under monotonic and uni-axial conditions, the equivalent von Mises stress is equal to the axial stress $\sigma$, and the axial plastic strain $\varepsilon_p$ is equal to the equivalent plastic strain $p$. The hardening law coupling the Chaboche model and a power law relates the uniaxial stress $\sigma$ to the equivalent plastic strain $p$in the viscoplastic regime, which is given by:

$$\sigma = \sigma_y + Q_1\left(1 - e^{-bp}\right) + Q_2 p + K_a \dot{p}^{1/N_a} \tag{5}$$

The parameters $\sigma_y$, $Q_1$, b, $Q_2$, $K_a$ and $N_a$are identified through a reverse engineering method using experimental data consisting of monotonic tensile tests performed on PA66 samples at RH50% and two different strain rates, namely $8\times10^{-2}$, and $8\times10^{-3}$ $s^{-1}$ [43]. Figure 22 shows the

correlation between the experimental and the simulated responses. The identified material parameters are listed in Table 5.

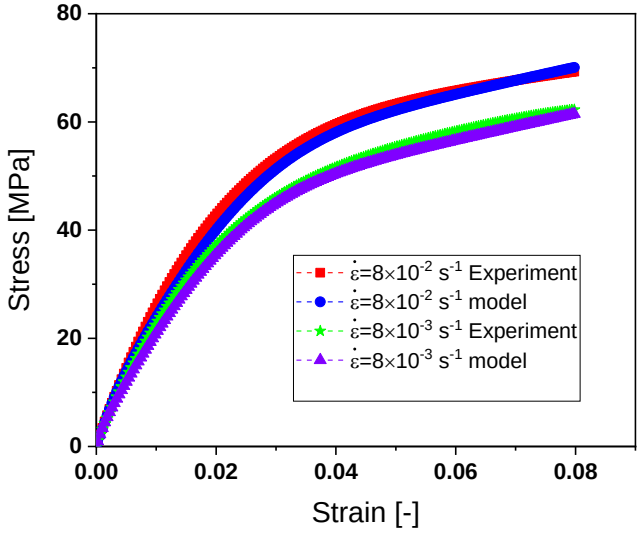


Figure 22: Calibration of the viscoplastic model of equation (5) using the experimental data from [44] for two strain rates.

Table 5: Identified elasto-viscoplastic material parameters of the PA66 at RH50% using experimental data [44]

| Polyamide matrix |
|---|
| $E(MPa) = 3000$ |
| $\vartheta = 0.34$ |
| $\sigma_y(MPa) = 1$ |
| $Q_1(MPa) = 39$ |
| $b = 134$ |
| $Q_2(MPa) = 260$ |
| $K_a\ (MPa.s^{1/Na}) = 45$ |
| $N_a = 2.37$ |

As mentioned in section 4.2, it is assumed that the fibers in each strand are orientated in the same direction, therefore the material properties of the strand (glass fiber and PA66 matrix) are calculated using the Mori-Tanaka scheme [39,40]. The properties are presented in table 6.

Table 6: Mechanical properties of the strand using a mean-field homogenization technique (Mori-Tanaka) [39,40]

| Strand |
|---|
| $E_{11}(MPa)$= 65101.99 |
| $E_{22} = E_{33}$ $(MPa)$ =29835.95 |
| $G_{12} = G_{13}(MPa) = 12217.65$ |
| $G_{23}(MPa)$ = 10901.29 |
| $\vartheta_{12} = \vartheta_{13}$= 0.26 |
| $\vartheta_{23}$= 0.36 |

FEA is performed to predict the elastic and the elastic-viscoplastic responses of the TP-ROS materials utilizing a multi-scaled bending model. Two cases have been analyzed: the first considers the matrix as an elastic media and the second assumes it as an elastic-viscoelastic polymer. There is approximately a 2 % error between the experimental and numerical results. For example, in case 2, the load rises linearly with increasing displacement as expected until the load is approximately 348 N at a displacement of 6.5 mm.

In terms of load-displacement curves, the comparison between the numerical simulation and experimental tests is shown in Figure 23, considering room temperature T=23°C and a relative RH equal to 50%. The numerical load-displacement curves predicted using the developed modeling strategy are very close to those obtained experimentally. This level of agreement is exhibited for both elastic and non-linear regimes of the overall response. It is worth mentioning that as a first attempt to numerically capture the effect of the microstructure, the non-linear part of the overall material response is assumed to be caused by only the viscoplasticity of the polymer matrix. The developed multiscale simulation strategy succeeds to capture the overall response of the sample under a 3-point bending configuration.

The differences between the experimental and numerical curves beyond the peak force in figure 23 can thus be explained by the fact that appropriate damage mechanisms have not been incorporated into the multiscale simulation. Due to the high local stiffness of the unidirectional strands, damage tends to initiate in the matrix-rich zones between the strands, which is driven by the viscoplastic nature of the matrix. The accumulation of this matrix degradation gives rise to delamination between the strands, leading to macroscopic failure of the specimen.

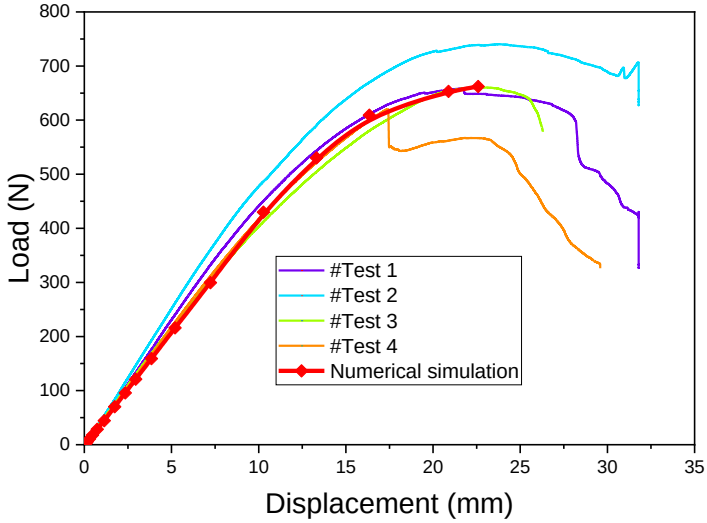


Figure 23: Comparison between experimental data from three-point flexural test and numerical results predicted using the developed multi-scale modeling strategy for TP-ROS composite, accounting for the viscoplastic regime of the PA66 matrix.

Figure 24 displays an overview of the displacement and the von Mises stress fields at the central region of interest of the flexural sample. The displacement and stress fields in the region of interest are non-uniform due to the complex and irregular mesostructure induced by the random distribution of the strands.

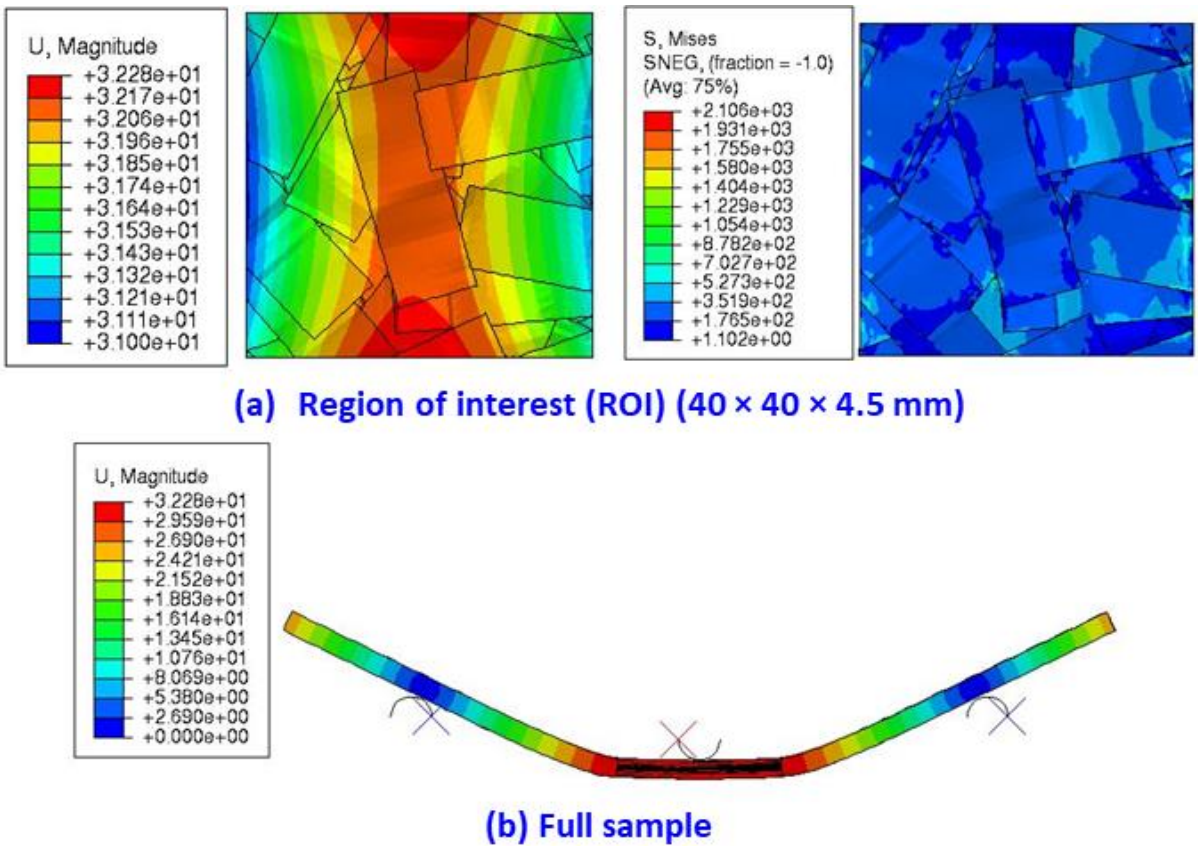


Figure 24: Numerical results showing the equivalent von Mises stress distribution and displacement fields of TP-ROS composite at the ROI and the full sample.

A sensitivity analysis has been conducted to highlight the effect of the strand length. Several RVEs ($40\times40\times4.5mm^3$ at $V_f$ = 47%) with varying strand lengths (L= 10 mm, 20 mm, 26 mm) but constant width (w=10 mm) have been built and discretized. Three FE models with different mesostructures have been designed and subjected to the same loading and boundary conditions, as presented in Section 3. The overall flexural load-displacement responses have been predicted for all RVEs, as illustrated in Figure 25 (a). The results indicate that the increase in strand length leads to a minor increase in the structural integrity of the TP-ROS composite in terms of the flexural stiffness and maximum load, as shown in Figure 25 (b). Similar results were also reported in the literature [49,50], highlighting the effect of the strand length on the overall mechanical properties.

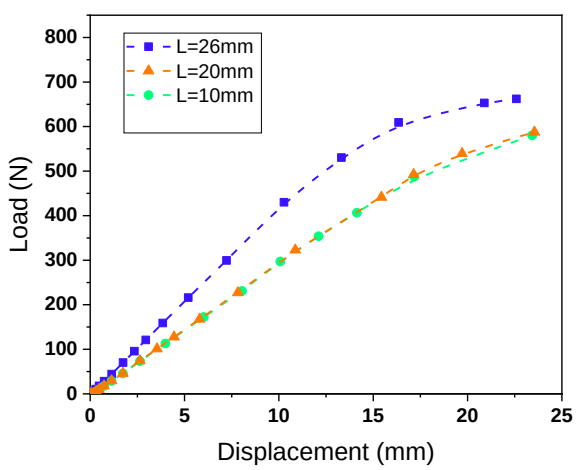


(a)

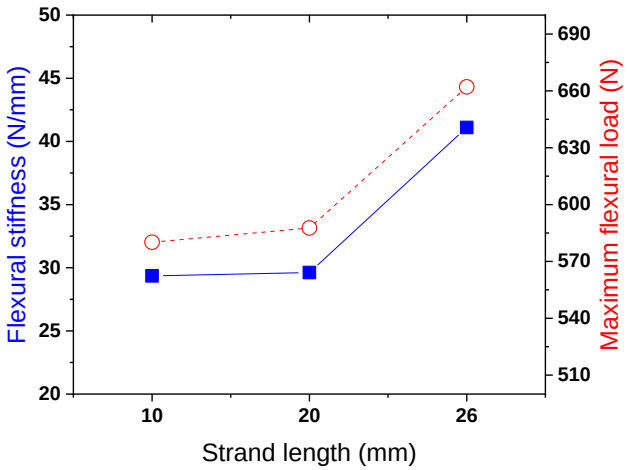


(b)

Figure 25: Numerical results showing the effect of strand length on the bending behavior of TP-ROS composite.

In addition, the von Mises stress distribution in the ROI presented in Figure 26 illustrates the effect of the strand length on the flexural behavior of the TP-ROS composite. It can be seen that the average local stress is reduced with an increase in strand length. On the other hand, the stress concentration is higher for the shortest strand, which can lead to a catastrophic macroscopic failure of the sample as observed in figure 13. These results prove the abilities of the proposed approach to investigate the relationship between microstructural parameters and mechanical performance for recycled thermoplastic composite materials.

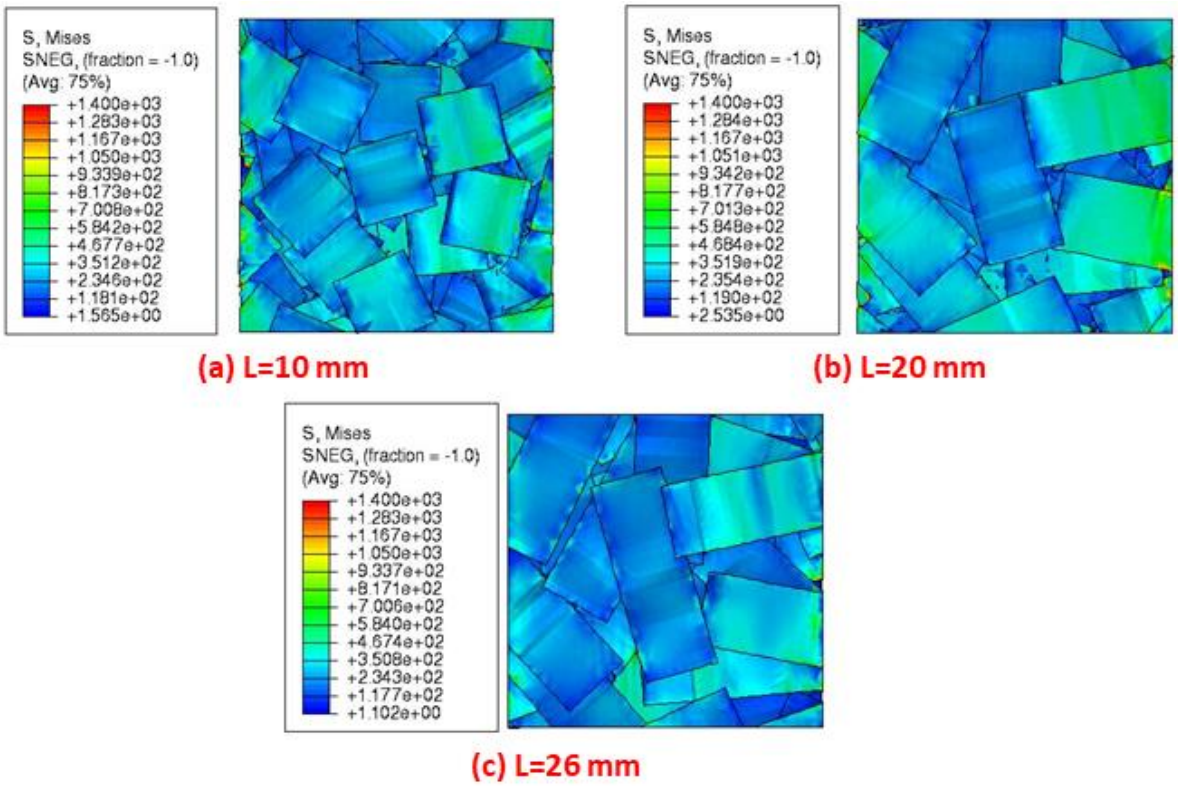


Figure 26. The contour of von Mises stress in the region of interest was computed for three mesostructures: Effect of strand length

Additional RVEs of 40×40×4.5 mm have been generated for three different volume fractions, namely: 20%, 30%, and 47%. Flexural stiffness and maximum load results as a function of volume fraction are presented in Figure 27. The effect of volume fraction appears to significantly influence stiffness and maximum load. Contour plots of von Mises stress are presented in Figure 28 to show the effect of fiber volume fraction.

From a mechanical properties standpoint, the obtained numerical results suggest that there is a possible compromise between fibre volume fraction and strand length, based on the limited number of samples examined in this research. Longer strands can introduce fabrication complexities due to a higher probability of fiber misalignment, as well as resin richness or unreinforced regions due to poor fibre strand homogeneity. High fibre volume fractions can also lead to fiber breakage, resulting in shorter fibres. Based on these results, the optimal strand length and fiber volume fraction can be selected based on manufacturing considerations and mechanical performance.

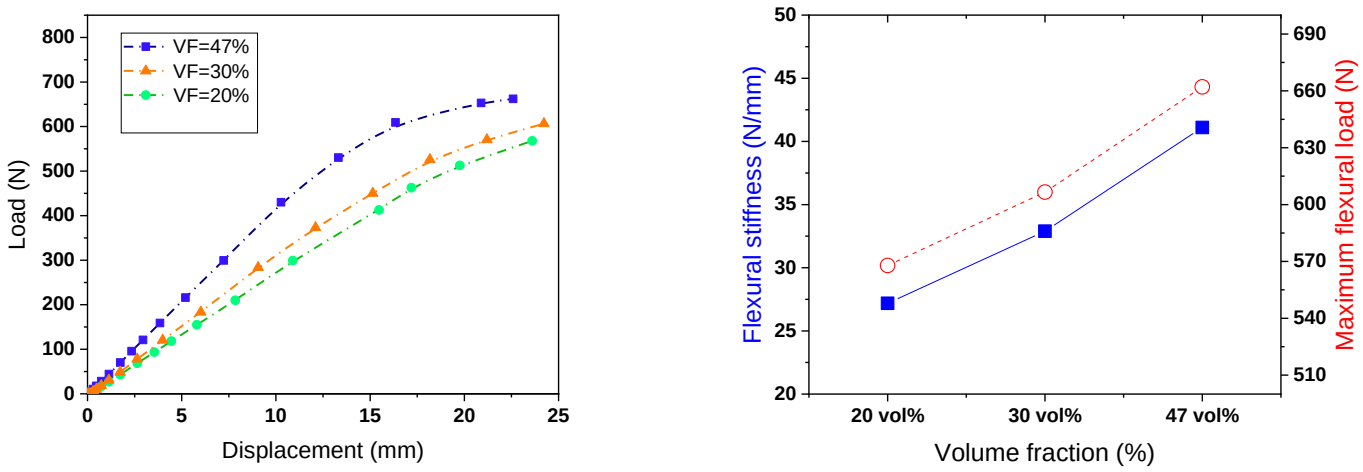


(a) (b)

604

605 Figure 27: Numerical results showing the effect of volume fractions on the bending
606 behavior of TP-ROS composite.

607

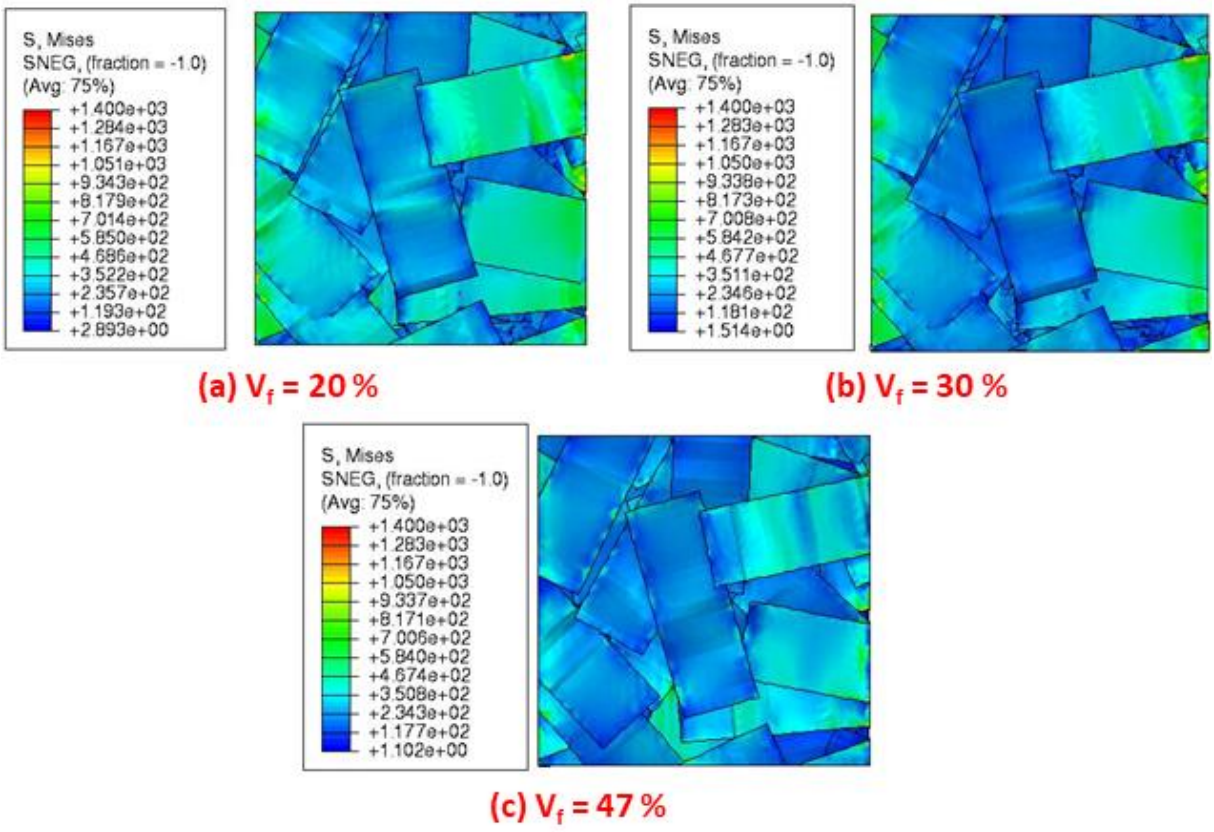


608

609 Figure 28. Contour plots of von Mises stress in the region of interest computed for three
610 mesostructure: Effect of fiber volume fraction

611

Overall, the capability of the model for capturing the influence of strand length and volume fraction on the mechanical performance of TP-ROS composite has been established. The modeling strategy is suitable for predicting the effect of the induced fibre microstructure on the mechanical response for random strand reinforced thermoplastics.

## 5. Conclusion and further work

In this research, a multiscale model was successfully used to study the influence of the microstructure on the mechanical properties of recycled glass fiber-reinforced thermoplastic composites. Panels abbreviated as TP-ROS were fabricated with chopped reinforcements using an innovative process developed by Cetim Grand Est. Based on a microstructural analysis, the reinforcement architecture of the recycled composite material is random and highly disordered. The strands are randomly distributed and exhibit varying patterns. This architecture is a result of the arbitrary deposition process combined with the local material flow during the thermo-compression molding process. The resulting material behavior has been analyzed at two different scales: the microscopic scale and the mesoscopic scale. The results from this multiscale analysis have highlighted the mechanical performance of the recycled composite material. A hybrid computational framework has been proposed for predicting the flexural properties, by isolating the effects of certain material parameters such as the volume fraction and size effect of the strands.

Although the only non-linearity of the global behavior has been assigned to the viscoplastic nature of the thermoplastic matrix, a good agreement is obtained between the numerical multiscale simulation and the experimental results. It supports the use of this technique as a first attempt for capturing the effect of the microstructure induced by the recycling process on the flexural performance of TP-ROS composite. Equally, the present multiscale modeling approach can be employed for other types of composites with similar microstructural features.

Whilst damage mechanisms have not been incorporated into the developed multiscale model, it still serves as a useful tool to better understand the effects of process-induced microstructural features on the mechanical response. Accordingly, several further aspects need to be addressed in future work. Firstly, an extended microstructural characterization of the recycled composite material needs to be performed to quantify the influence of the fiber orientation distribution induced by material flow within the mold tool. Secondly, damage mechanisms need to be incorporated to track the initiation and accumulation of damage up until

macroscopic failure of the TP-ROS material. Several models have been developed by the authors considering ductile damage of thermoplastic matrix, fiber/matrix debonding as well as strand damage induced by transverse cracking and pseudo-delamination [51,52].

## Declaration of Competing Interest

The authors declare that they have no known competing financial interests or personal relationships that could have appeared to influence the work reported in this paper.

## Acknowledgments

This work was partially supported by the French Region Grand Est, and the European Community (#AL0029234). The author from the University of Nottingham also gratefully acknowledges the support from the Engineering and Physical Sciences Research Council, as part of the "EPSRC Future Composites Manufacturing Research Hub" (EP/P006701/1).

## References

[1] Nachtane, M., Tarfaoui, M., Goda, I., & Rouway, M. (2020). A review on the technologies, design considerations, and numerical models of tidal current turbines. Renewable Energy, 157, 1274-1288.

[2] Fitoussi, J., Bocquet, M., & Meraghni, F. (2013). Effect of the matrix behavior on the damage of ethylene–propylene glass fiber reinforced composite subjected to high strain rate tension. Composites Part B: Engineering, 45(1), 1181-1191.

[3] Krauklis, A. E., Karl, C. W., Gagani, A. I., & Jørgensen, J. K. (2021). Composite material recycling technology—state-of-the-art and sustainable development for the 2020s. Journal of Composites Science, 5(1), 28.

[4] Oliveux, G., Dandy, L. O., & Leeke, G. A. (2015). Current status of recycling of fibre reinforced polymers: Review of technologies, reuse and resulting properties. Progress in materials science, 72, 61-99.

[5] Rybicka, J., Tiwari, A., & Leeke, G. A. (2016). Technology readiness level assessment of composites recycling technologies. Journal of Cleaner Production, 112, 1001-1012.

[6] Gonçalves, R. M., Martinho, A., & Oliveira, J. P. (2022). Recycling of reinforced glass fibers waste: Current status. Materials, 15(4), 1596.

[7] Henshaw, J. M., Owens, A. D., Houston, D. Q., Smith, I. T., & Cook, T. (1994). Recycling of a cyclic thermoplastic composite material by injection and compression molding. Journal of Thermoplastic Composite Materials, 7(1), 14-29.

[8] Colucci, G., Ostrovskaya, O., Frache, A., Martorana, B., & Badini, C. (2015). The effect of mechanical recycling on the microstructure and properties of PA66 composites reinforced with carbon fibers. Journal of Applied Polymer Science, 132(29).

[9] Kiss, P., Stadlbauer, W., Burgstaller, C., Stadler, H., Fehringer, S., Haeuserer, F., & Archodoulaki, V. M. (2020). In-house recycling of carbon-and glass fiber-reinforced thermoplastic composite laminate waste into high-performance sheet materials. Composites Part A: Applied Science and Manufacturing, 139, 106110.

[10] Mengeloglu, F., & Karakus, K. (2008). Thermal degradation, mechanical properties and morphology of wheat straw flour filled recycled thermoplastic composites. Sensors, 8(1), 500-519.

[11] Grigorescu, R. M., Ghioca, P., Iancu, L., David, M. E., Andrei, E. R., Filipescu, M. I., ... & Bucurica, I. A. (2020). Development of thermoplastic composites based on recycled polypropylene and waste printed circuit boards. Waste Management, 118, 391-401.

[12] Barnett, P. R., Gilbert, C. L., & Penumadu, D. (2021). Repurposed/recycled discontinuous carbon fiber organosheet development and composite properties. Composites Part C: Open Access, 4, 100092.

[13] Vincent, G. A., de Bruijn, T. A., Wijskamp, S., Rasheed, M. I. A., van Drongelen, M., & Akkerman, R. (2019). Shredding and sieving thermoplastic composite scrap: Method development and analyses of the fiber length distributions. Composites Part B: Engineering, 176, 107197.

[14]Visweswaraiah, S. B., Selezneva, M., Lessard, L., & Hubert, P. (2018). Mechanical characterisation and modelling of randomly oriented strand architecture and their hybrids–A general review. Journal of Reinforced Plastics and Composites, 37(8), 548-580.

[15]Harper, L. T., Qian, C. C., Luchoo, R., & Warrior, N. A. (2017). 3D geometric modelling of discontinuous fiber composites using a force-directed algorithm. Journal of Composite Materials, 51(17), 2389-2406.

[16]Pan, Y., Iorga, L., & Pelegri, A. A. (2008). Analysis of 3D random chopped fiber reinforced composites using FEM and random sequential adsorption. Computational Materials Science, 43(3), 450-461.

[17]Tang, H., Zhou, G., Chen, Z., Huang, L., Avery, K., Li, Y., ... & Su, X. (2019). Fatigue behavior analysis and multi-scale modelling of chopped carbon fiber chip-reinforced composites under tension-tension loading condition. Composite Structures, 215, 85-97.

[18]Harban, K. (2015). Stiffness and Strength Predictions of Discontinuous Fiber Composites (Doctoral dissertation).

[19]Kravchenko, S. G., Sommer, D. E., Denos, B. R., Avery, W. B., & Pipes, R. B. (2019). Structure-property relationship for a prepreg platelet molded composite with engineered meso-morphology. Composite Structures, 210, 430-445.

[20] Kravchenko, S. G., Sommer, D. E., Denos, B. R., Favaloro, A. J., Tow, C. M., Avery, W. B., & Pipes, R. B. (2019). Tensile properties of a stochastic prepreg platelet molded composite. Composites Part A: Applied Science and Manufacturing, 124, 105507.

[21] Kilic, M. H. (2014). A nonlinear 3D micromechanical and structural framework for analysis of discontinuous long-fiber thermoplastic composites. CAMX–The composites and advanced materials expo.

[22] Benaarbia, Adil, André Chrysochoos, and Gilles Robert. "Thermomechanical behavior of PA6. 6 composites subjected to low cycle fatigue." Composites Part B: Engineering 76 (2015): 52-64.

[23] Chen, Qiang, George Chatzigeorgiou, and Fodil Meraghni. "Extended mean-field homogenization of viscoelastic-viscoplastic polymer composites undergoing hybrid progressive degradation induced by interface debonding and matrix ductile damage." International Journal of Solids and Structures 210 (2021): 1-17.

[24] Miqoi, Nada, et al. "Detection and evaluation of barely visible impact damage in woven glass fabric reinforced polyamide 6.6/6 composite using ultrasonic imaging, X-ray tomography and optical profilometry." International Journal of Damage Mechanics 30.3 (2021): 323-348.

[25] Arif, M. F., Saintier, N., Meraghni, F., Fitoussi, J., Chemisky, Y., & Robert, G. (2014). Multiscale fatigue damage characterization in short glass fiber reinforced polyamide-66. Composites Part B: Engineering, 61, 55-65.

[26] Arif, M. F., Meraghni, F., Chemisky, Y., Despringre, N., & Robert, G. (2014). In situ damage mechanisms investigation of PA66/GF30 composite: Effect of relative humidity. Composites Part B: Engineering, 58, 487-495.
[27] https://www.cetimgrandest.fr/notre-rd-recyclage-des-materiaux-polymeres-et-composites-thermoplastiques/
[28] Siegmund, T., Cipra, R., Liakus, J., Wang, B., LaForest, M., & Fatz, A. (2004). Processing-Microstructure-Property Relationships in a Short Fiber Reinforced Carbon-Carbon Composite System. In Mechanics of Microstructured Materials (pp. 235-258). Springer, Vienna.
[29] Phelps, J. H. (2009). Processing-microstructure models for short-and long-fiber thermoplastic composites. University of Illinois at Urbana-Champaign.
[30] Bargmann, S., Klusemann, B., Markmann, J., Schnabel, J. E., Schneider, K., Soyarslan, C., & Wilmers, J. (2018). Generation of 3D representative volume elements for heterogeneous materials: A review. Progress in Materials Science, 96, 322-384.
[31] Rasheed, M. A., Rietman, B., Visser, H. A., & Akkerman, R. (2013). Experimental characterisation of recycled (glass/TPU woven fabric) flake reinforced thermoplastic composites. In Proceedings of the 19th International Conference on Composite Materials Iccm. Montreal, Canada.
[32] Vincent, G. A., de Bruijn, T. A., Wijskamp, S., Rasheed, M. I. A., van Drongelen, M., & Akkerman, R. (2021). Characterisation and improvement of the quality of mixing of recycled thermoplastic composites. Composites Part C: Open Access, 4, 100108.
[33] Bhakta, A., Ali, W., Geijselaers, H. J. M., Sachs, U., Rasheed, M. I. A., & van den Boogaard, A. H. (2017, August). Effect of flake distribution in mold on the flow during compression molding of unidirectional long fiber thermoplastic flakes. In 21st International Conference on Composite Materials 2017.
[34] Miqoi, Nada, et al. "Ultrasonic and X-Ray tomography inspection of a woven glass reinforced composite damaged by fatigue loading." The Journal of the Acoustical Society of America 144.3 (2018): 1785-1785.
[35] Pomarede, P., Meraghni, F., Peltier, L., Delalande, S., & Declercq, N. F. (2018). Damage evaluation in woven glass reinforced polyamide 6.6/6 composites using ultrasound phase-shift analysis and X-ray tomography. Journal of Nondestructive Evaluation, 37(1), 1-21.
[36]Selezneva, M. and L. Lessard. Characterization of mechanical properties of randomly oriented strand thermoplastic composites. Journal of Composite Materials: p. 1-19, 2015.
[37] Selezneva, M., et al. Modelling of Mechanical Properties of Randomly Oriented Strands Thermoplastic Composites. ECCM16 - 16th European Conference On Composite Materials, Seville, Spain, 2014.
[38] Harper, L. T., Qian, C. C., Luchoo, R., & Warrior, N. A. (2017). 3D geometric modelling of discontinuous fiber composites using a force-directed algorithm. Journal of Composite Materials, 51(17), 2389-2406.
[39] Benveniste, Y. (1987). A new approach to the application of Mori-Tanaka's theory in composite materials. Mechanics of materials, 6(2), 147-157.
[40] Desrumaux, F., Meraghni, F., & Benzeggagh, M. L. (2001). Generalised Mori-Tanaka scheme to model anisotropic damage using numerical Eshelby tensor. Journal of Composite Materials, 35(7), 603-624.
[41] Luchoo, R., Harper, L. T., Warrior, N. A., & Dodworth, A. (2011). Three-dimensional numerical modelling of discontinuous fiber composite architectures. Plastics, rubber and composites, 40(6-7), 356-362.
[42]Harper, L. T., Qian, C., Turner, T. A., Li, S., & Warrior, N. A. (2012). Representative volume elements for discontinuous carbon fiber composites–Part 1: Boundary conditions. Composites Science and Technology, 72(2), 225-234.

[43] Praud, F., Chatzigeorgiou, G., Bikard, J., & Meraghni, F. (2017). Phenomenological multi-mechanisms constitutive modelling for thermoplastic polymers, implicit implementation and experimental validation. Mechanics of Materials, 114, 9-29.
[44] Barral, M., Chatzigeorgiou, G., Meraghni, F., & Léon, R. (2020). Homogenization using modified Mori-Tanaka and TFA framework for elastoplastic-viscoelastic-viscoplastic composites: Theory and numerical validation. International Journal of Plasticity, 127, 102632.
[45] Tikarrouchine, E., et al. "Non-linear FE2 multiscale simulation of damage, micro and macroscopic strains in polyamide 66-woven composite structures: analysis and experimental validation." Composite Structures 255 (2021): 112926.
[46] Chaboche, J.L., 1989. Constitutive equations for plasticity and viscoplasticity. International Journal of Plasticity 5, 247-302.
[47] Chaboche, J.L., 2008. A review of some plasticity and viscoplasticity constitutive theories. International Journal of Plasticity 24, 1642-1693.
[48] Lemaitre, J., Chaboche, J.L., 1994. Mechanics of solid materials. Cambridge University Press.
[49] Feraboli, P., Peitso, E., Deleo, F., Cleveland, T., & Stickler, P. B. (2009). Characterization of prepreg-based discontinuous carbon fiber/epoxy systems. Journal of reinforced plastics and composites, 28(10), 1191-1214.
[50] Horn, B., Neumayer, J., & Drechsler, K. (2018). Influence of strand length and thickness on strength and stiffness of stranded laminates. Journal of Composite Materials, 52(16), 2199-2212.
[51]Chen, Q., Chatzigeorgiou, G., Robert, G., & Meraghni, F. (2022). Viscoelastic-viscoplastic homogenization of short glass-fiber reinforced polyamide composites (PA66/GF) with progressive interphase and matrix damage: New developments and experimental validation. Mechanics of Materials, 164, 104081.
[52] Praud, F., Chatzigeorgiou, G., & Meraghni, F. (2021). Fully integrated multi-scale modelling of damage and time-dependency in thermoplastic-based woven composites. International Journal of Damage Mechanics, 30(2), 163-195.